

High-energy cosmic gamma rays probe the most energetic phenomena in nature. The diverse list of known sources includes active galactic nuclei (AGN), which are believed to be powered by accretion onto super-massive (10^6 – 10^9 solar mass) black holes; high-energy cosmic rays interacting with other matter in the galaxy; the diffuse extragalactic background, whose origin is still not determined; supernovae and their remnants, which are likely sites of cosmic-ray acceleration; and gamma-ray bursts, arguably the most powerful — and still unexplained — events in the universe. One of the defining characteristics of many of these sources is that they are highly transient, with timescales ranging from $10\ \mu\text{s}$ to $1000\ \text{s}$ for gamma-ray bursts, to days for AGN flares. In addition, these remarkable systems are often observed to emit most of their power at GeV and higher energies, with ~ 10 -TeV gammas observed from one AGN source, Mkn 501 (Protheroe et al. 1997).

Beyond these known but not yet well understood sources is a diverse list of hypothetical sources possibly awaiting discovery, including particle dark matter annihilations and decays, and other relics from the Big Bang such as cosmic strings (a consequence of gauge theories not testable with terrestrial accelerators) and evaporating black holes. What is common to these diverse sources is that all of the fundamental interactions in nature, including gravity, play an important role in concert in an extreme environment.

As we emphasize in this section, observations of gamma rays in the GLAST energy range ($20\ \text{MeV}$ to $300\ \text{GeV} \rightarrow 1\ \text{TeV}$) *combined* with a significantly larger field of view, highly efficient duty cycle, superior pointing and energy resolutions, and long lifetime provide a unique and compelling opportunity to answer definitively a wealth of questions — and at the same time to open up major discovery opportunities.

To set the stage, the EGRET all-sky survey map of gamma rays with $E > 100$ MeV is shown in Figure 2.a-1 in galactic coordinates. Although the variability is not represented, the richness of the gamma-ray sky is otherwise apparent. The most obvious features are:

1. The extra-galactic diffuse flux (the mainly blue regions far outside the galactic disk). This flux is approximately 1.5×10^{-5} photons $\text{cm}^{-2}\text{s}^{-1}\text{sr}^{-1}$;
2. The galactic diffuse flux, approximately two orders of magnitude larger; and
3. Galactic and extra galactic point sources, including pulsars, AGNs, and sources not yet associated with observations in other wavelengths. The typical point source flux observable by EGRET is $O(10^{-7}-10^{-6})$ photons $\text{cm}^{-2}\text{s}^{-1}$.

We now outline some of the physics associated with each of these features, and the power of the GLAST instrument to address these topics.

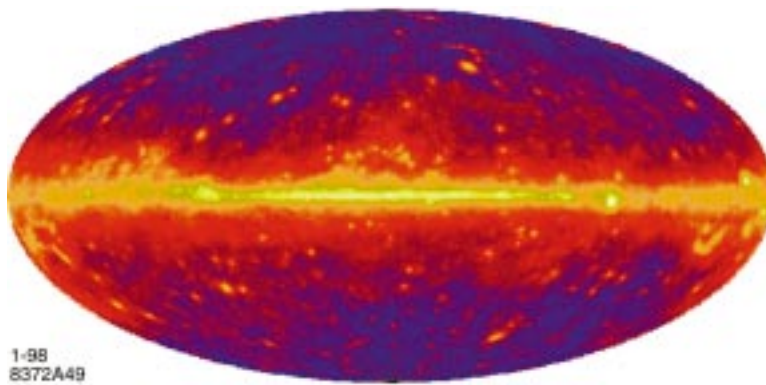


Figure 2.a-1 EGRET all-sky map in galactic coordinates for $E_\gamma > 100$ MeV.

NB: Throughout this section we refer to the GLAST “scanning mode.” In this mode of observation, GLAST is zenith-pointing as it circles in orbit, likely with a slight north/south rock to allow full-sky coverage including the poles. Pointed modes may also be used, but at this time we expect the scanning mode to dominate GLAST observations for the first few years of on-orbit operations.

2.A Active Galactic Nuclei

Active galaxies probably represent the largest class of high-energy gamma-ray emitters, and identify sites where extreme particle acceleration is taking place. Blazars are flat-radio-spectrum AGNs, whose members include BL Lac objects and highly polarized and optically violently variable quasars. Their associated jets also commonly exhibit superluminal motion (Vermeulen & Cohen 1994). The currently favored models of blazars (Blandford & Rees 1978; Blandford & Königl 1979. For reviews see Rees 1984; Begelman, Blandford, & Rees 1984) qualitatively explain observed characteristics in wavelengths from radio to the highest energy gamma rays (~ 10 TeV). These models posit that we are viewing these objects almost down the throat of a highly collimated jet of relativistic particles emanating from “a central engine,” putatively an accreting supermassive black hole—mass in the range 10^6 – $10^9 M_\odot$. Such jets are seen in high detail via radio maps of these sources.

Blazars are incredibly powerful and highly variable. They have been observed to emit as much as $\sim f \times 10^{49}$ ergs/sec in gammas over the energy range of 100 MeV to 5 GeV (von Montigny et al. 1995; Mukherjee et al. 1997); f is the solid angle subtended by the AGN jet $\sim 10^{-3}$ (beaming factor of ~ 1000) in some popular models. The beaming of photons is required if they are not to be absorbed via $\gamma\gamma \rightarrow e^+e^-$ on their way out from the source (Maraschi et al. 1992; Mattox et al. 1993; McNaron-Brown et al. 1995; Dermer & Gehrels 1995).

In electron-positron jet models the main source of the high-energy gamma rays is the Compton up-scattering of low-energy photons by the high-energy, very non-thermal electrons and positrons in the jet. There are two classes of models for the source of soft photons. In the synchrotron self Compton (SSC) models the source is synchrotron radiation produced by the high-energy electrons themselves. In the external radiation Compton (ECR) models, either the accretion disk (~ 10 eV) (Dermer, Schlickeiser, & Mastichiadis 1992), or the emission line clouds and/or intercloud medium provides the photons (Sikora, Begelman, & Rees 1994; Blandford & Levinson 1995). For an example of a recent comparison of this type of model to multiwavelength data, see Dermer, Sturmer, & Schlickeiser 1997.

Note that it is still controversial whether the jets are primarily made of an electron-positron plasma or an electron-proton plasma (Celotti & Fabian 1993). While the observed multi-wavelength spectra are reasonably represented by the electron-positron models for the blazars, there is a very inter-

esting possibility that proton-initiated cascades contribute substantially in some blazars (Mannheim & Biermann 1992). In the electron-proton version, π^0 production and decay play important parts in the very high-energy gamma-ray spectrum.

One of the great successes of the Compton Gamma Ray Observatory (CGRO) mission has been the studies of active galaxies. Over 50 blazar-type AGNs have been detected by the EGRET instrument alone (Mukherjee et al. 1997). Variability timescales as short as hours have been observed by EGRET for $E_\gamma > 100$ MeV (Hartman et al. 1992; Kniffen et al. 1993).¹ EGRET has observed these objects to redshifts of over two, and radio observations indicate that they extend to redshifts of four or more (von Montigny et al 1995; Mukherjee et al. 1997).

A second and important class of gamma-ray emitting AGNs is known as Seyfert galaxies. About seventeen of these galaxies — which tend to be much nearer in distance to the Milky Way than blazars, and so more evolved — have been detected mainly by another CGRO instrument, OSSE (Webb 1997). In the theoretical unified view of gamma-ray emission from AGNs, Seyferts differ from blazars in part because we are viewing them from a different angle, so that we are looking through the galaxy rather than looking down the jet as in the case of blazars. This unified model initially found support from observations by the Japanese x-ray satellites Ginga and ASCA (Mushotzky et al. 1993). For Seyferts, in this model, the jet emission is not pointing at us and thus is less important than emission more closely associated with the inner regions of the galaxy itself. Data from the OSSE instrument in the high-energy x-ray to MeV regime, combined with Ginga and ASCA observations in the x-ray, find that the average spectrum of the Seyfert galaxies is well described by this sort of picture. Unexpectedly, the Seyfert energy spectrum falls off much more quickly than previously thought. Previous observations suggested that Seyfert emission extended up to the MeV range. (See Section 2.A.3, page 2-12, for a quantitative discussion of the angular dependence on viewing angle.) The average Seyfert spectrum indicates otherwise. Figure 2.a-2 shows an artist's conception of an AGN based on current models that naturally explain many of the AGN characteristics described above.

¹ Significant sub-day variability has been observed by the Japanese x-ray satellite ASCA in the x-ray band (Takahashi et al. 1996) and by ground-based groups at very high energy (Protheroe et al. 1997).

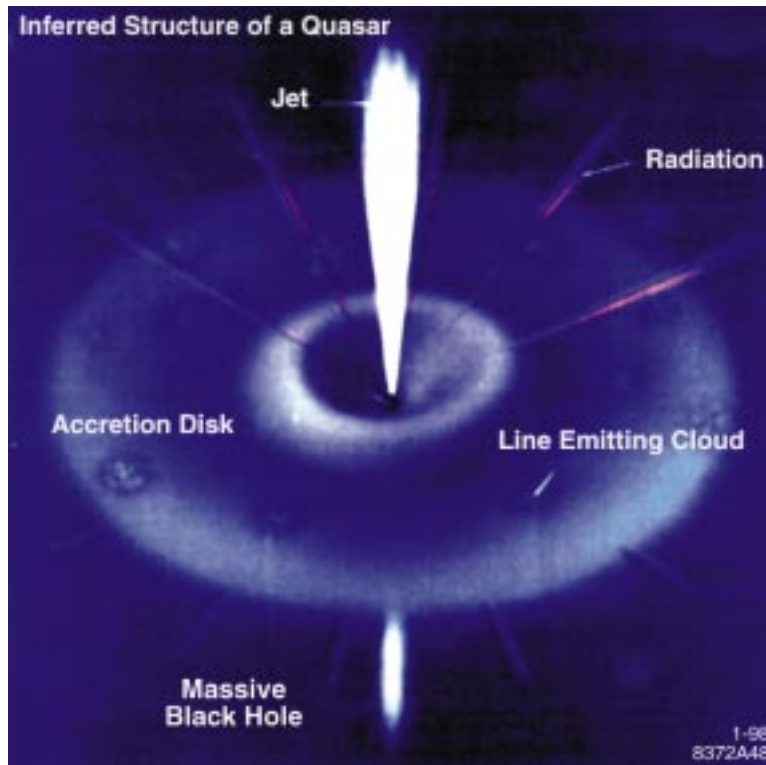


Figure 2.a-2 Artist's impression of an AGN powered by black hole central engine based on current models.

2.A.1 Source Search

GLAST will dramatically extend the number of observed AGNs, as well as the energy range over which they can be observed. Indeed, GLAST might be called the “Hubble telescope” of gamma-ray astronomy as it will be able to observe AGN sources to redshifts of $z \cong 4$, that is, to the time of their formation.

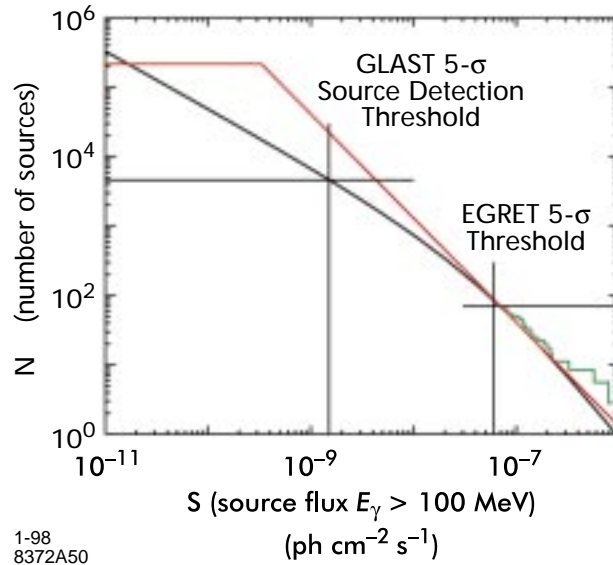


Figure 2.a-3 A $\log N$ vs. $\log S$ relation for gamma-ray sources showing the two orders of magnitude increase in known sources expected from GLAST. The model gamma-ray sky is constructed with a galactic diffuse model derived from EGRET data and an AGN model of the diffuse gamma-ray background.

Figure 2.a-3 shows the $\log N$ vs. $\log S$ relation for AGNs, where S is the source flux for $E_\gamma > 100$ MeV and N is the number of sources with flux $\geq S$. The black curve is extrapolated from EGRET data and an AGN model of the diffuse gamma-ray background based on the assumption that AGN sources follow a luminosity function similar to flat-spectrum radio quasars (Dunlop & Peacock 1990; Willis 1997; also see Stecker & Salamon 1996). The red curve shows the Euclidean extrapolation of the EGRET distribution. It is cut off so as not to conflict with the observed isotropic diffuse radiation level. Extrapolation from EGRET AGN detections using the black curve projects that about 5000 AGN sources will be detected in a four-year cumulative scanning mode observation by GLAST, as compared to the 50 or so that have been observed by EGRET in a similar time interval.

Figure 2.a-4 compares a one-year all-sky map of EGRET data with a Monte Carlo simulation of a one-year all sky survey with GLAST. The figure shows a blowup of the Virgo region of the sky as viewed by EGRET and GLAST. What we see with the GLAST simulation in the blowup of the Virgo region is a stellar-like field of AGN in >1 -GeV gamma rays. Note that GLAST will measure the typical AGN position on the sky to arc-minute accuracy, thus facilitating association with an optical and/or radio counterpart.

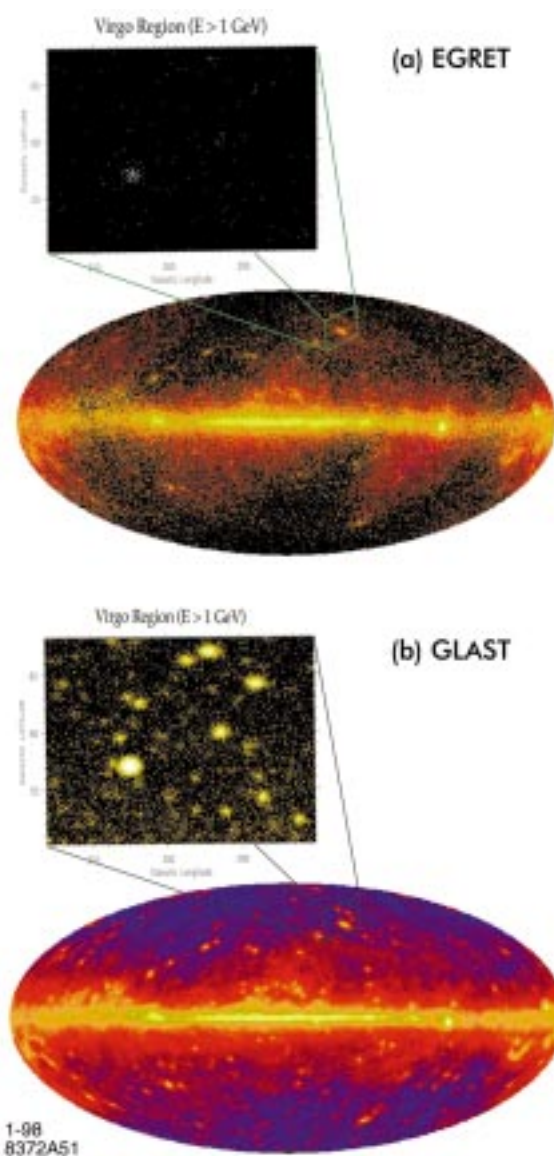


Figure 2.a-4 a. EGRET data one-year all-sky map ($E_\gamma > 100$ MeV), with blowup of Virgo region ($E_\gamma > 1$ GeV).
 b. GLAST Monte Carlo simulation of one-year all-sky map in scanning mode ($E_\gamma > 100$ MeV), with blowup of Virgo region ($E_\gamma > 1$ GeV).

In addition to observing vast numbers of AGNs in their quiescent state, GLAST will be an AGN transient detector. GLAST is a unique observatory to monitor the variability of thousands of AGNs. Past limited observations have observed violent eruptions with time scales of hours. There are also hints of long-term variability over years. Many interesting physical processes will manifest themselves through the systematic multi-wavelength monitoring of AGN transient behavior over the entire sky.

2.A.2 AGN Energy Spectra for Observation Close to 0° to the Jet — Standard Blazar

The wideband spectra of blazars have two pronounced components: one broad peak at low energies (LE) extending from IR to soft x-ray, and a second broad peak at high energies (HE) in the gamma-ray band.

Blazars that are hosted in quasars (QHBs in, for example, OVV quasars) and radio-selected BL Lac objects (RBLs or LBLs) typically have the LE peak in the IR band. On the other hand the majority of BL Lac objects and x-ray selected BL Lacs (XBLs), have the LE peak in the UV or soft x-ray bands. The high level of polarization observed from radio to UV implies that the LE component is most likely produced via synchrotron radiation in a macroscopic scale magnetic field. The luminosity ratio of the HE to LE components is systematically larger for QHBs than for XBLs, and the Lorentz factors of electrons contributing to the peak in the $\nu F(\nu)$ spectrum (ergs/sec/cm² at the instrument) is much lower for QHB than for XBL, despite the fact that magnetic field is comparable in the QHB and XBL (Kubo et al. 1997).

Figure 2.a-5 shows the energy spectrum of the blazar Mkn 421 from radio wavelengths to about 2 TeV. Power per cm², in Jy-Hz (Jansky-Hz) is plotted vs. energy in MeV of the observed gamma-ray flux (at the instrument). Note that $1 \text{ Jy-Hz} \equiv 10^{-23} \text{ erg-s}^{-1}\text{-cm}^{-2}$.

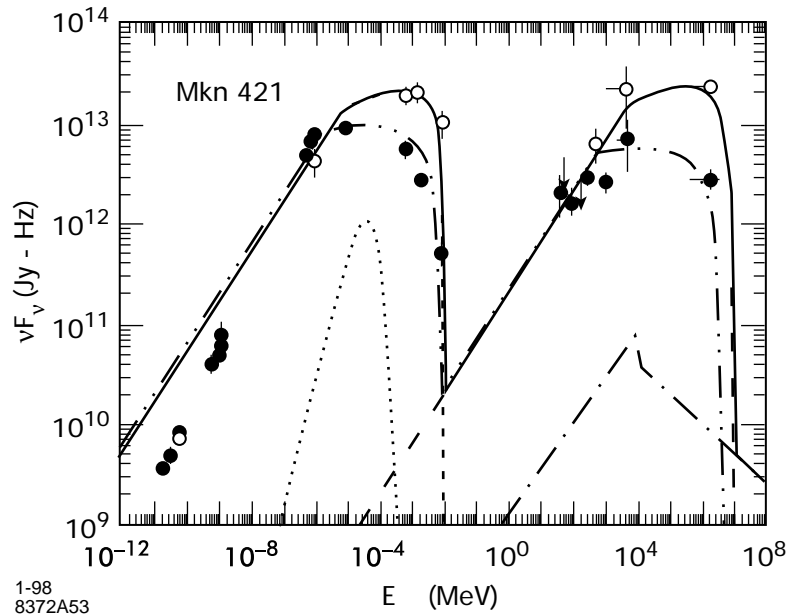


Figure 2.a-5 Filled data points and upper limits show measurements of the quiescent flux of Mkn 421, and open data points show measurements of Mkn 421 within two days of the May 15, 1994 TeV flare. Mkn 421 is at $z = 0.031$. Triple dot-dashed (quiescent) and solid curves (flare) give the results of the model fit of Dermer et al. 1997, assuming equipartition between energy densities for the magnetic field and external soft photons, with other parameters given in the reference. The synchrotron (short dashed), disk (dotted), synchrotron self Compton (dot dashed), and external Compton scattering (long dashed) components are shown separately for the quiescent state. The data points were obtained from Macomb et al. 1995, while the model fits are from Dermer, Sturmer, & Schlickeiser 1997.

Figure 2.a-6 shows the energy spectrum of the quasar 3C273 from radio wavelengths to 500 GeV. The data were obtained from Lichti et al. 1995, while the model fits are from Dermer, Sturmer, & Schlickeiser 1997.

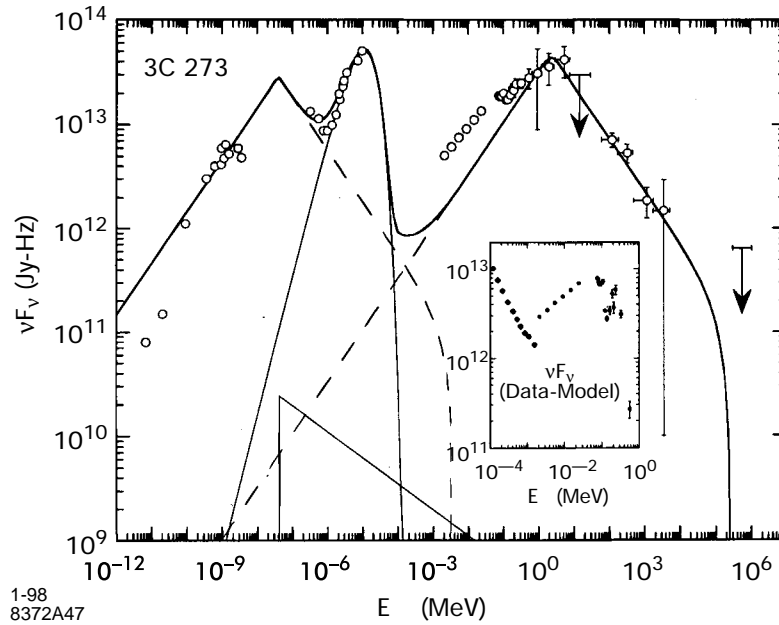


Figure 2.a-6 Measurements and upper limits for the multiwavelength campaign of 3C273 during June 15–28, 1991 (Lichti et al. 1995). 3C273 is at $z=0.158$, much further than Mkn 421. The solid curve gives the results of the model fit of Dermer et al. 1997, assuming equipartition between energy densities for the magnetic field and external soft photons, with other parameters given in the reference. The synchrotron (lowest energy dashed curve), accretion disk radiation (sharply peaked solid curve) synchrotron self Compton (lower triangular shaped curve), and external Compton scattering (highest energy dashed curve) components are shown separately. The inset shows the difference spectrum between the x-ray/gamma-ray data and the model fit, with non-simultaneous Rosat x-ray data also included. The excess emission is attributed to an incomplete treatment of accretion disk radiation (Dermer et al. 1997).

Nearby AGNs, for example, Mkn 501 and 421 ($z \sim 0.03$) show spectra to multi-TeV energies, while more distant AGN, e.g., 3C273 ($z=0.158$), show spectral cutoffs in the 4 GeV–0.5 TeV range. However, the physical mechanisms responsible for cutoffs in the energy spectrum of AGNs vs. z are not yet determined. EGRET measurements typically lose sensitivity at >10 GeV (depending on the strength of the source), while the ground-based Cherenkov telescopes currently have a threshold of about 0.5 TeV, with expectations to move to the 100–200 GeV range and perhaps lower. The lower threshold is limited by background, see Section 2.F (page 2-43). Thus, for currently well-measured sources, there is an unexplored region between about 10 GeV to about 500 GeV due to past experimental limitations. From a combination of EGRET and ground-based Cherenkov telescope measurement it appears certain that

this unexplored energy band, ~ 10 to ~ 100 GeV, holds interesting surprises. As Figure 2.a-7 shows, GLAST is being designed to have good sensitivity in this band.

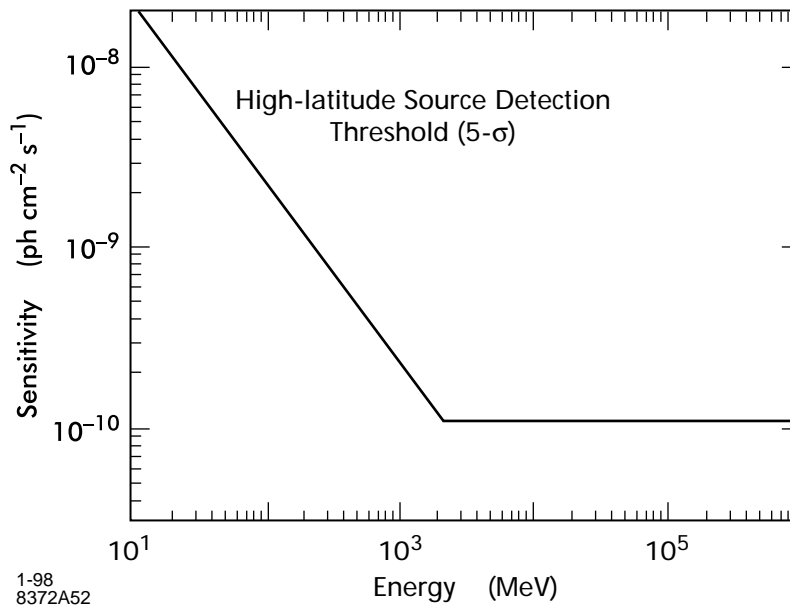


Figure 2.a-7 High-latitude point source detection threshold for GLAST one-year all-sky survey. GLAST integrated point source sensitivity in photons/cm²/sec is plotted vs. observed photon energy in MeV. The curve assumes GLAST is in the scanning mode over a year, and an integrated high latitude diffuse gamma ray background of $2 \times 10^{-5} \times (100 [\text{MeV}] / E_{\gamma} [\text{MeV}])^{1.1}$ [photons/cm²/sec/sr], consistent with EGRET observations. The source is assumed to have a $1/E_{\gamma}^2$ distribution, typical of many EGRET sources. Thus the minimum source gamma flux is calculated for achieving a five-sigma point source detection over background for $E_{\gamma} > \text{Energy}$ for a year in scanning mode, e.g., the required source flux at the instrument to obtain a five-sigma detection, in a year of scanning mode, at high latitude, for > 100 MeV is 3×10^{-9} ph/cm²/sec.

What is the reason for the cutoff in the AGN energy spectrum? The Dermer et al. models assume a source-intrinsic cutoff, and fit to determine model parameters that are source-specific. Figures 2.a-5 and 2.a-6 show that reasonable, if not perfect, fits to the existing data can be obtained this way, but there are many fitted parameters (in addition to the lack of data between ~ 10 GeV and ~ 500 GeV) needed to achieve a factor of ~ 100 difference in intrinsic cutoff energy between Mkn 421 and 3C273. Another explanation for cutoffs in this energy range is that they have a cosmological origin, namely interaction with the extra galactic background light, or EBL. Only by observ-

ing many examples of AGNs over a wide range of redshifts can one hope to untangle these two possible sources of cutoff. GLAST measurements, combined with ground-based Cherenkov telescope measurements, of the spectral cutoffs of a very large sample of AGNs covering a redshift range from $z \sim 0.03$ to up to a $z \sim 4$ will both untangle intrinsic AGN spectral cutoffs from EBL absorption effects, and probe and map the EBL. (These observations require the association of AGNs with optical counterparts which greatly benefits from the arc-minute positional information from GLAST.)

The EBL was produced by galaxies undergoing starbursts during the epoch of galaxy formation. The absorption of high-energy gamma rays occurs over cosmological distance via $\gamma\gamma \rightarrow e^+e^-$ interactions with near-ultraviolet, optical and near-infrared photons that make up the EBL. The cross section for this interaction is maximized when $\varepsilon \approx (1/3) \times (1 \text{ TeV}/E)$ [eV], where ε is the EBL photon energy in eV, and E is the gamma-ray energy in TeV. Figure 2.a-8 shows how an unabsorbed AGN spectrum would appear if observed at redshifts of $z=0.5$ and 2 for particular EBL models (Madau & Phinney 1996; also see Salamon & Stecker 1997). Determination of the EBL can provide unique information on the formation of galaxies at early epochs, and will test models for structure formation in the universe, such as those in which a neutrino mass of 5 to 10 eV plays an important role (e.g., see Macminn & Primack 1995).

2.A.3 Angular Distribution of AGN Emission and Corresponding Energy Dependence

GLAST may have the sensitivity to probe further the incredible engine that drives the AGN acceleration process by observing AGNs whose jets are not pointing at the earth to within a few degrees. Figure 2.a-9 shows the time-averaged spectral power flux at different observing angles θ to the jet axis from AGN model calculations (Dermer, Sturmer, & Schlickeiser 1997; see also Sambruna et al. 1996). This result comes from time-averaging a time-dependent simulation. Energies represented in the figure range over 20 orders of magnitude, from 10^{-12} MeV, or radio wavelengths, to 10^8 MeV=100 TeV. To achieve this range of energies for the critical testing of AGN models necessitates GLAST observations of AGN simultaneously with radio, optical, and x-ray observatories.

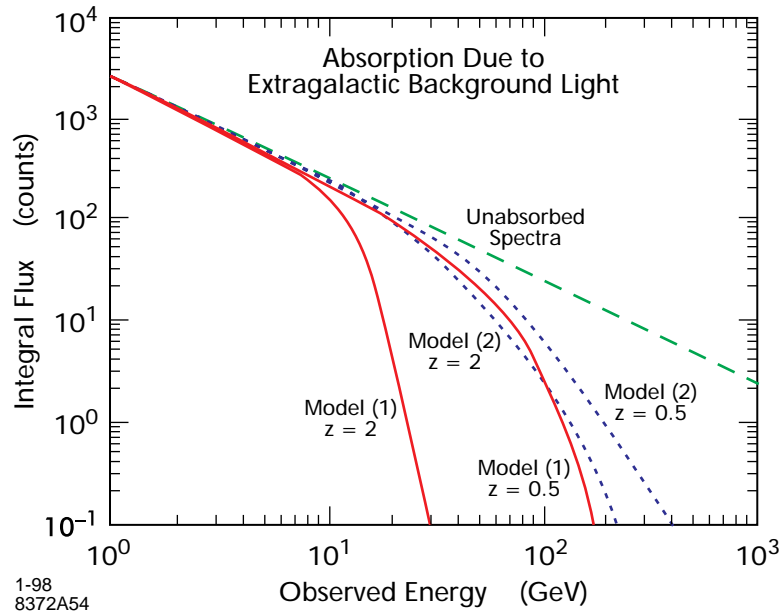


Figure 2.a-8 High-energy gamma-rays emitted by distant AGNs can interact with EBL photons before they have a chance to reach us. Shown above is how an unabsorbed AGN spectrum would appear if observed at redshifts of $z = 0.5$ and 2 for two particular EBL models (based on Madau & Phinney 1996). GLAST observations of the high-energy spectra for a large sample of AGN at various redshifts will map out the EBL. The ordinate of the graph is in arbitrary units.

To give the reader a feeling for the results shown for the AGN model fits, a brief description of the Dermer et al. AGN jet model follows. The calculation gives the instantaneous spectral power flux and the time-integrated spectral power fluence produced as a function of energy of the observed gammas and the angle of these gammas to the jet direction.

Relativistic electrons are injected into an on-axis jet blob moving away from a central black hole of mass M (solar masses), with bulk Lorentz factor $\Gamma \sim 10$. Additional assumptions have the electrons instantaneously injected into the comoving blob frame with an isotropic angular distribution and a $1/E_e^2$ electron energy distribution, with $1 < E_e/m_e < 10^5$ (m_e the mass of the electron). The jet blob radius is r_b , assumed to be spherical in the comoving frame, and the blob consists of a thermal electron-positron plasma with density $n_{th} = (\sigma_T \times r_b)^{-1}$, where σ_T is the Thomson (inverse Compton scattering) cross section. (Note that in the calculations the blob length is scaled to 1000 gravitational radii $= 10^3 \times 1.5 \times 10^5 [\text{cm}] \times M$.) The derivation of the high-energy pho-

ton fluences is restricted to the regime where either synchrotron radiation losses or inverse Compton scattering losses with photons from the external radiation field dominate the electron energy loss rate and hence the photon production from the jet.

The magnetic field permeating the region of photon production is estimated at 1 Gauss, which drives the synchrotron radiation photon production from the electron beam. Also, the electron jet is moving through a radiation field, which drives the inverse Compton scattering, that is, up-scattering photon production. The radiation field is assumed in the calculation to be a 10 eV monochromatic, spherical radiation field (Sikora et al. 1994), with total inverse Compton scattering depth τ^s ($\tau_{-2}^s \equiv \tau^s/100$), surrounding the supermassive black hole ($M_g \equiv M[\text{solar masses}]/10^8[\text{solar masses}]$). A description of the actual central engine energy source mechanism is not included. There is also a scale distance for the radiation field from the black hole, R_{sc} ($R_{0.1} \equiv R_{sc}[\text{pc}]/0.1[\text{pc}]$). The intensity of the external photon field is given by equation 33 from Dermer et al. (1997) as $4.3 \times 10^3 \times (I_{Edd} \times M_g \times \tau_{-2}^s / R_{0.1}^2)$, where the luminosity of this accretion photon field is written in terms of the normalized Eddington limit luminosity, I_{Edd} ($I_{Edd} \equiv L_{disk}[\text{ergs/sec}] / (1.26 \times 10^{46} \times M_g)$ [ergs/sec]).

The model calculation presented in Figure 2.a-9 takes, $I_{Edd} = M_g = \tau_{-2}^s = R_{0.1} = 1$. The AGN is placed at $z=1$. The power going into the jet is set equal to the Eddington luminosity. The figure shows the time-averaged spectral power flux at different observing angles for the model and parameters described in the previous paragraphs.

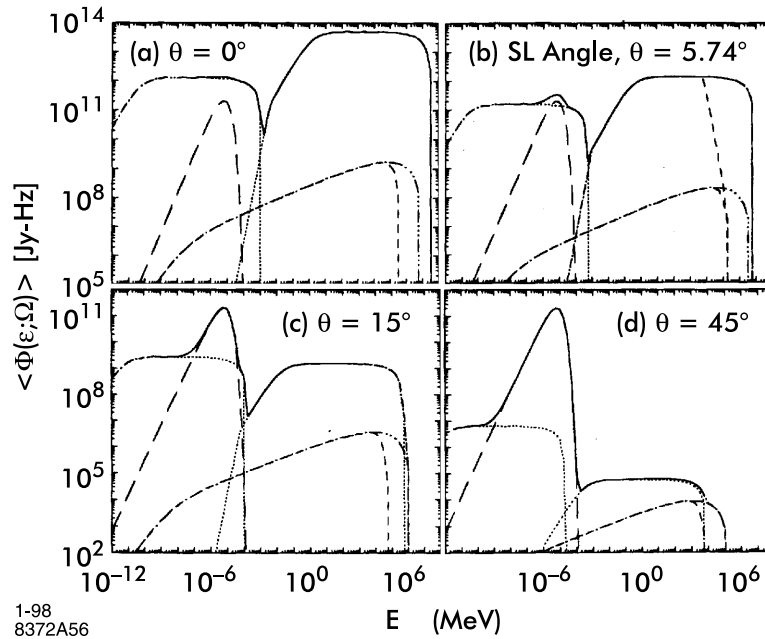


Figure 2.a-9 Model of AGN emission at various angles to the jet axis (Dermer et al. 1997). Time-averaged spectral power flux in Jy-Hz is plotted vs. E in MeV. (A description of the model is provided in the text.) The long dashed curves show the accretion-disk flux, the dotted curves at low and high energies are the synchrotron and external Compton scattering components, respectively, and the dot-dashed curves are the synchrotron self-Compton components. Note the relative contributions of the beamed jet and the low-energy quasi-isotropic disk components, and that the spectra cutoff at about 35 TeV for 0° , 8 TeV for 5.74° , 1 TeV for 15° , and 0.1 TeV for 45° .

Using this model, Bloom & Wells (1997) have estimated the off-axis luminosity for two very nearby AGNs, Centaurus A at 2 Mpc and M87 at 12 Mpc (NB: $z=0.03$ is ~ 120 Mpc, see Zombeck 1990). They find that M87 with a jet axis angle of $42 \pm 5^\circ$ with respect to the earth direction may show an observable signal in GLAST above ~ 10 GeV. At lower energies the diffuse background will dominate. Centaurus A has a jet axis of about 68° with respect to the earth direction, and should show no observable signal. By sampling AGNs with different jet axis directions with respect to the earth directions as determined by radio measurements, GLAST may be able to considerably constrain AGN models such as the one presented in Figure 2.a-9.

2.A.4 Unidentified EGRET Sources

The discovery by SAS-2 and COS-B of a number of gamma-ray luminous sources provided one of the first mysteries of gamma-ray astrophysics, and one that remains largely unsolved. Here is a set of prominent sources that have high gamma-ray/x-ray and high gamma-ray/optical luminosity ratios, making any identification difficult. Although most of the early detections were of galactic sources, the EGRET catalogs have extended the puzzle to all parts of the sky (Thompson et al. 1995, 1996). Over 60% of the sources seen by EGRET (more than 150 in the latest catalog, Hartman et al. 1998) remain unidentified. Like other high-energy gamma-ray sources, they are some sort of astrophysical particle accelerator with an environment that allows the conversion of particle energy into radiation. What sort of accelerator? By analogy with known sources, some may be pulsars or blazars that are hidden from other wavelength observations, though not all share the characteristics of the hypothesized parent populations. Figure 2.a-10 shows the distribution of the EGRET unidentified sources on the sky, along with other classes of sources.

Little is known about the unidentified sources, but some general properties can be derived from their spatial and luminosity distributions. At least two groups of unidentified sources are seen: a group clustered along the galactic plane, possibly associated with sites of star formation such as OB associations; and a high galactic latitude group that is statistically non-isotropic, having an excess toward the galaxy that suggests a nearby population mixed with a distant one (Grenier 1997).

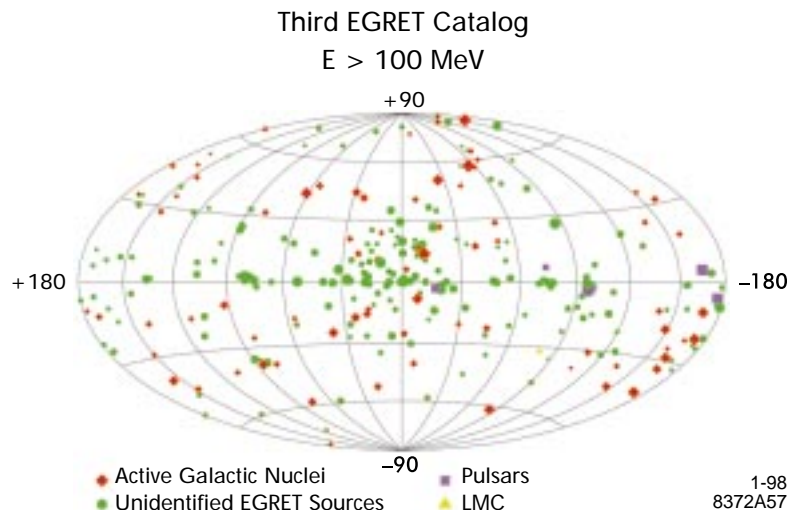


Figure 2.a-10 Map of EGRET point sources in galactic coordinates for $E > 100 \text{ MeV}$.

GLAST will be the breakthrough instrument for unraveling this mystery or mysteries. For the first time, a gamma-ray telescope will have the combination of sensitivity and resolution to tie the gamma-ray sources to specific objects. How GLAST will accomplish this goal will depend on what the sources turn out to be. Here are some of the possibilities:

- **Previously unknown blazar-class AGNs.** Some of these have probably already been found. The unidentified source 2EG J0432+2910, for example, was identified with a radio/optical/infrared source that has the characteristics of a BL Lac object, following the detection of a gamma-ray flare during a high state of the radio emission (Lundgren et al. 1995). The wide field of view and high sensitivity of GLAST will catch such flares readily; the arc-minute error boxes will then allow comparison with a manageable number of radio and optical sources to search for correlated flaring activity. Using gamma rays to find new blazars is an important step toward understanding the collective properties (such as evolution on cosmological time scales) of this class.
- **Previously unknown pulsars.** Two of the unidentified COS-B sources turned out to be pulsars — Geminga and PSR B1706-44. It would be remarkable if Geminga were the only radio-quiet pulsar, and indeed pulsar models predict that more pulsars should be visible in gamma rays without strong radio emission (Yadigaroglu and Romani 1995). GLAST will use two approaches to find such pulsars: first, for the brighter sources (including many if not most of the EGRET sources) GLAST will have the ability to find pulsations in the gamma-ray data, independent of observations at other wavelengths; and second, for the weaker sources the small error boxes will allow deep x-ray searches for the expected pulsed thermal emission (the method used to find Geminga). The methods and implications of such discoveries are discussed further in Section 2.D (page 2-37) on pulsars.
- **Binary systems.** 2EG J0241+6119 (2CG135+01) is consistent in position with the variable radio source GT0236+610, also seen in optical and x-rays and thought to be a binary system. Particles may be accelerated by shocks at the boundaries between strong winds from the two companions (Kniffen et al. 1997). Recently, EGRET has seen evidence for GeV gamma-ray emission from the well-known x-ray binary Centaurus X-3, indicating that at least some of these high-mass x-ray binary systems can accelerate particles at least some of the time

(Vestrand et al. 1997). Accurate positioning of the sources and spectral measurements are critical to confirming these identifications. Because all such sources are time-variable, GLAST will be well suited to monitoring them, using the wide field of view.

- **Something new.** Two possibilities emerge from the EGRET results. 2EG J1835+5919 is a source seen repeatedly by EGRET, but no x-ray or radio counterpart has been found to suggest either a blazar or pulsar origin (Nolan et al. 1996). Though it might still be a pulsar with an x-ray source too weak to detect with present telescopes, it may be a different type of object entirely. The persistent source 2EG J1746-2852, which is associated with the galactic center (Mayer-Hasselwander et al. 1998) is also a mystery. Among the suggestions for the origin of this source is advection onto the putative black hole at the center of our galaxy. A different type of EGRET source, GRO J1838-04, was detected as a transient, flaring for only a few days, reminiscent of a blazar and very unlike the pulsars, which are always visible. There is, however, no flat-spectrum radio source in the error box nearly as strong as most blazars seen by EGRET. This is probably the best candidate for an astrophysical accelerator of a new type (Tavani et al. 1997). GLAST's high resolution, broad energy range, and wide field of view all come into play for such sources. The small error box allows deep searches at other wavelengths; the broad energy range gives a spectrum that can be used to study directly the physical processes involved in producing the gamma rays; and the wide field of view permits GLAST to track the time history of such sources for long stretches, in order to correlate any variability with sources found in the deep images in other wavebands.

In thinking about the unidentified EGRET sources, the example of the gamma-ray bursts before the Compton observatory (CGRO) may be a useful reference point. Before CGRO, there was a near consensus that the gamma-ray bursts were rather ordinary flashes associated with nearby neutron stars. Nevertheless, BATSE was included in the payload, just to verify the predictions. The results are well-known: the BATSE bursts now seem quite astounding phenomena, likely coming from cosmological distances and involving prodigious energies. The lesson is clear — an unknown class of objects always has the potential for the most remarkable discoveries.

2.B The Diffuse Gamma-ray Background

An apparently isotropic, hence extra-galactic, component of the diffuse gamma-ray flux was discovered by the SAS-2 satellite (Thompson & Fichtel 1982) for energies $E=30\text{--}150$ MeV. The energy spectrum in this range was well determined, but the isotropy was poorly established due to low statistics. What is responsible for this flux of gamma rays? There are a number of possibilities. The most prosaic, and thus perhaps the most likely, is composite light from a large number of faint point sources, such as AGNs (Stecker & Salamon 1996). Other more exotic possibilities, which imply exciting particle physics, are relics from some yet-unknown high-energy process in the early universe (see Section 2.B.1, page 2-20), such as neutralino decay in R -parity violating versions of SUSY in the early universe.

Through the era subsequent to COS-B, when 3C273 was the only extragalactic point source detected, the composite AGN light hypothesis could not be tested. More point sources had to be characterized so that an extrapolation of their intensity and energy distributions could be attempted. Study of the isotropic flux was greatly advanced with EGRET, due to its lower instrumental background, and greater sensitivity. Dozens of extra-galactic sources have been detected (Thompson et al. 1995; von Montigny et al. 1995), and most have been identified with the blazar class of AGNs. Sreekumar et al. (1997) have analyzed the uniformity and spectrum of the isotropic flux. Removal of the contributions from resolved point sources remains a difficulty, due to the large size of the EGRET point spread function. The foreground galactic flux, mostly originating from cosmic ray interactions with interstellar nuclei and photons, also must be subtracted carefully. The results indicate that the energy spectrum of the isotropic emission is well described by a power law, E^α , with spectral index $\alpha=-2.1\pm0.3$ over EGRET's energy range. The emission appears to be isotropic, at least on the $\sim 30^\circ$ angular scales of the study, although the systematic uncertainties are still fairly large. This value of α is consistent with the average index for blazars that EGRET has detected, which lends some support to the hypothesis that the isotropic flux is from unresolved blazars. The actual source fraction is difficult to measure, but has recently been estimated to be approximately 75% (Chiang & Mukherjee 1997). This finding depends sensitively on poorly-known parts of the gamma-ray luminosity function for blazars (Chiang et al. 1995).

GLAST will vastly increase the numbers of detected point sources, with a high-latitude flux limit about two orders of magnitude better than that of EGRET. Whereas EGRET has identified about 50 AGNs, GLAST should see more than 5000 as described in Section 2.A (page 2-3), thus resolving a greater fraction of the isotropic emission and permitting the blazar luminosity function at gamma-ray energies to be much better determined. GLAST will have much more uniform exposure at high latitudes, and because the sensitivity will not vary with time (unlike EGRET), the large-scale isotropy of the diffuse emission will be much better determined (Willis 1997).

After this definitive measurement, any truly diffuse component that remains would be of great interest, and would likely rank as one of the most important discoveries of GLAST.

2.B.1 Deep Survey of High-latitude Diffuse Background — Search for Signatures of Unstable Particle Relics (from $z < 700$) of the Big Bang

An extragalactic diffuse gamma-ray component could be the result of gamma emission from decays of exotic particles in the early universe. The energy spectrum of this component should be different from the AGN contributions. Again, the significantly larger effective area of GLAST, especially at high energies, may make the detection of this variance statistically significant (Kamionkowski 1995; Willis 1997), as shown in Figure 2.b-1.

There has been recent work on bounds on long-lived relics using EGRET and Comptel observations on the diffuse gamma-ray background (Kribs and Rothstein 1997). Many models predict long-lived relics that may or may not be dark matter candidates. Long lifetimes for heavy relics, where “long” means within several orders of magnitude of the age of the universe, may arise in models which have symmetries that are only broken at short distances, for example, technibaryons in technicolor models or the lightest supersymmetric partner in an R -parity violating supersymmetric extension of the standard model.

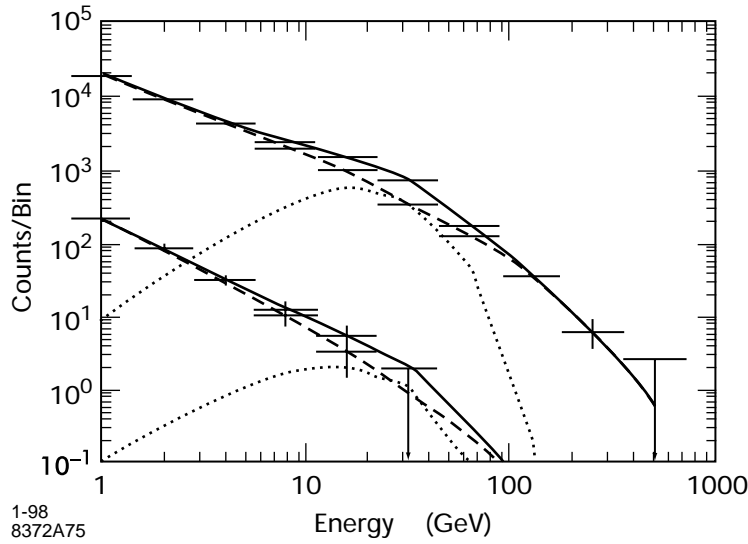


Figure 2.b-1 Simulated diffuse extra-galactic gamma ray flux measurements for GLAST (upper points) and EGRET (lower points). The dashed lines show the flux from unresolved AGNs, the dotted lines the contributions from WIMP decays in the early universe, and the solid line shows the total (Willis 1997).

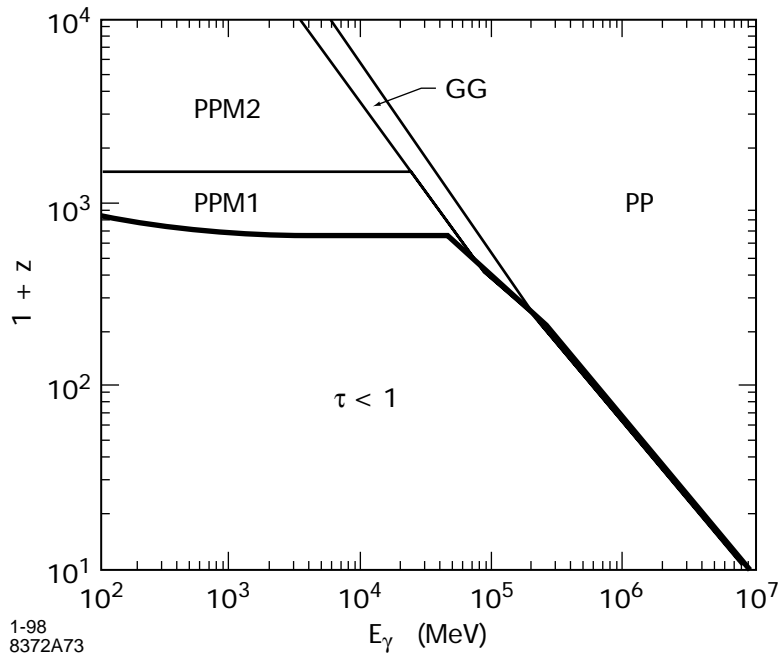


Figure 2.b-2 Dominant scattering mechanisms for high-energy photons injected in the post-recombination era. The region below the solid line has an optical depth $\tau < 1$, thus no scattering occurs. The other regions are dominated by e^+e^- pair production (PP), photon-photon scattering (GG), pair production in matter (PPM) and pair production in ionized matter (PPM2) (Kribs and Rothstein 1997).

Figure 2.b-2 shows the dominant scattering mechanisms for high-energy photons injected in the post-recombination era of the universe. This figure shows that the universe is essentially transparent to $z \sim 700$ for $100 \text{ MeV} < E_\gamma < 100 \text{ GeV}$, neglecting scattering from the EBL (which has been discussed in Section 2.A). Note that injection of a gamma of $< 300 \text{ GeV}$ at a $z > 100$ corresponds to $E_\gamma < 15 \text{ GeV}$ at $z \sim 5$, the beginning of the era of galactic formation. This implies that the EBL will negligibly absorb such photons.

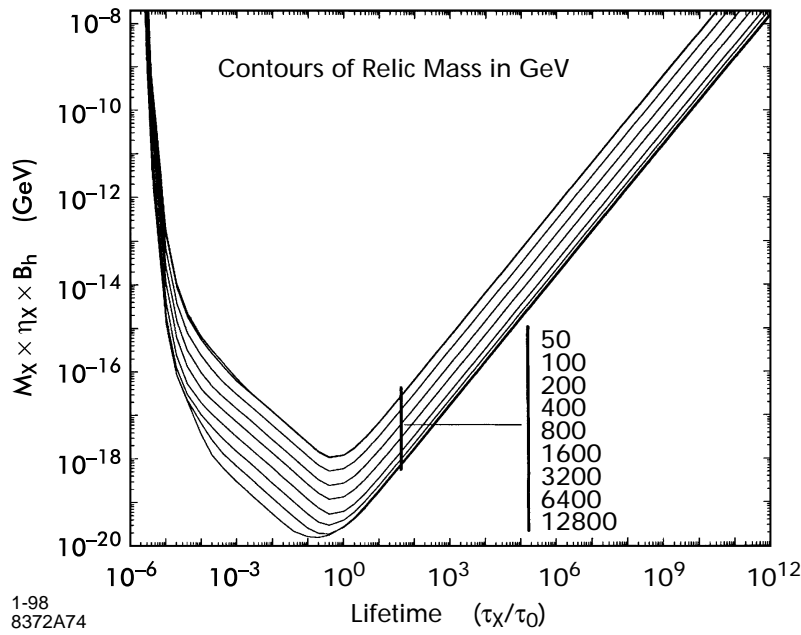


Figure 2.b-3 The final relic density bound for three-body hadronic decays with lifetimes in the indicated range. These bounds are obtained from Comptel and EGRET measurements of the extragalactic diffuse background. The bound scales linearly with the hadronic branching fraction of the relic, B_h , although a branching fraction different from 1 does not strongly affect these bounds. The upper limit on the relic density, $M_X \cdot \eta_X \sim 2 \times 10^{-8} \text{ GeV}$ is roughly the critical density corresponding to $\Omega_X h^2 \sim 1$. (Kribs and Rothstein 1997).

Figure 2.b-3 shows final relic density bounds for three-body radiative decays with lifetimes in the indicated range as obtained from analysis of the EGRET and Comptel measurements of the gamma-ray extra galactic diffuse background. In the figure $M_X \cdot \eta_X \cdot B_h [\text{GeV}]$ is plotted vs. τ_X / τ_0 , where M_X is the mass of the relic, η_X is the ratio of the relic to photon number density in the universe, B_h is the branching ratio for $X \rightarrow 3\text{-hadrons}$, τ_X is the relic lifetime and finally, τ_0 is the lifetime of the universe, $\sim 10^{10}$ years. Assuming that the relic has roughly the critical density, this analysis shows that lifetimes in the range

$3 \times 10^4 \text{ years} < \tau_{\tilde{\chi}} < (3 \times 10^{21} \rightarrow 3 \times 10^{23}) \text{ years}$, for masses $M_{\tilde{\chi}} = 50 \text{ GeV} \rightarrow 10 \text{ TeV}$, are excluded (compare to proton lifetime limits of $> 10^{33} \text{ years}$). In addition, relics with densities considerably below the critical density are excluded, which places a strong constraint on models with a long-lived massive particle.

GLAST measurements should improve these limits by at least two orders of magnitude. This improvement is expected due to the much larger energy range and sensitivity of GLAST as compared to EGRET, as well as the ability of GLAST to remove the point source contributions to the extragalactic gamma-ray “diffuse” background.

2.B.2 Gamma-ray Lines from Supersymmetric Particle Dark Matter Annihilation

The dark matter puzzle is currently one of the most interesting challenges confronting particle astrophysics and cosmology. The measured rotation curves of galaxies and galactic structure formation arguments are powerful evidence for dark matter in the universe. Evidence for dark matter in galaxies and the universe is reviewed in Ashman 1992 and Trimble 1989, respectively. Also see Kamionkowski & Spergel, 1994, for recent structure formation arguments.

The lightest supersymmetric particle (LSP), $\tilde{\chi}$, is a reasonable, and perhaps the most promising, candidate for the dark matter of the universe (Weinberg 1983; Goldberg 1983). It is neutral (hence the name neutralino), and stable if R parity is not violated. Supersymmetry seems to be a necessity in superstring theory (and M-theory) which potentially unites all the fundamental forces of nature, including gravity. If the scale of supersymmetry breaking is related to that of electroweak breaking, $\Omega_{\tilde{\chi}}$ may be the right order of magnitude to explain the non-baryonic dark matter. Although the highest energy accelerators have begun to probe regions of SUSY parameter space, the limits set at this time are not very restrictive. With the requirement that neutralinos make up most of the dark matter, current limits allow viable models in the mass interval, $30 \text{ GeV} < M_{\tilde{\chi}} < 10 \text{ TeV}$. (For an extensive review of the dark matter candidates and the experimental situation see Jungman, Kamionkowski, & Griest 1996.)

If neutralinos make up the dark matter of our galaxy, they would have non-relativistic velocities. Hence, the neutralino annihilation into the $\gamma\gamma$ and γZ final states can give rise to gamma rays with unique energies, that is, gamma-

ray lines with $E_\gamma = M_\chi$ or $E_\gamma = M_\chi(1 - m_Z^2/4M_\chi^2)$. The neutralino signal in its various guises has been thoroughly discussed in the literature (Jungman, Kamionkowski, and Griest 1996 and references therein, and more recently, Bergström, Ullio, & Buckley 1997). GLAST can search for gamma-ray lines in the mass above from 30 GeV thanks to its excellent energy resolution, $\sigma_E/E \sim 1.5\%$, for gamma rays entering for angles $>56^\circ$ from the normal. (Particles entering with angles $>56^\circ$ from the normal to the face of the GLAST instrument transverse >18 rl of CsI.)

Recently, full one-loop calculations of the $\chi\chi \rightarrow \gamma\gamma$ (Bergström & Ullio 1997; Bern et al. 1997) and $\chi\chi \rightarrow \gamma Z$ (Ullio & Bergström 1998) annihilation processes have been performed for the first time in the minimal supersymmetric extension of the standard model (MSSM). Figure 2.b-4 illustrates the complexity of the calculation. Compared to older estimates, the new computed rates are up to an order of magnitude larger. In particular, even TeV neutralinos have a remarkably strong coupling to these final states.

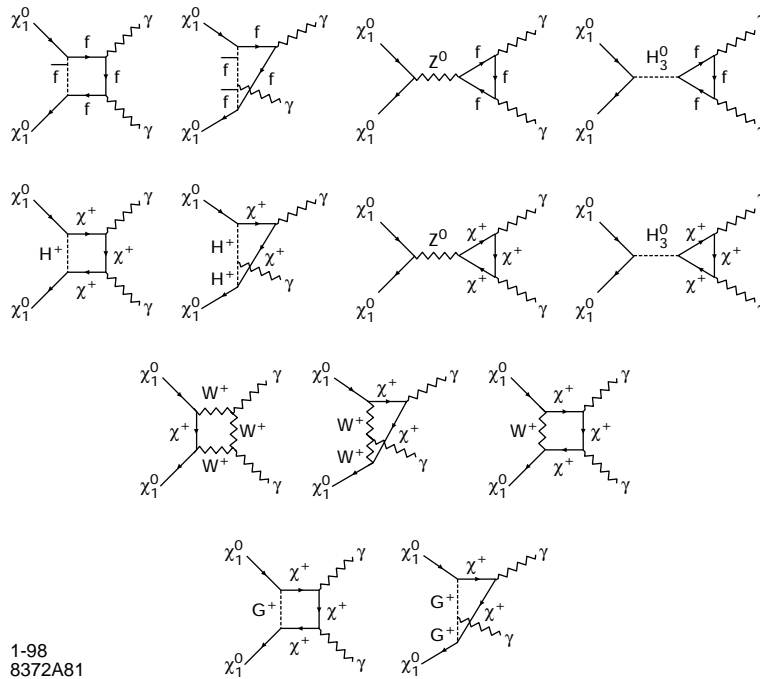


Figure 2.b-4 The Feynman diagrams contributing to neutralino annihilation into $\gamma\gamma$ (Bergström & Ullio 1997).

Different models have been proposed for the distribution of the halo dark matter in our galaxy. Recent n -body simulations of dark matter halos have, however, given indications of a universal profile where the density increases substantially near the galactic center region, the NFW halo model (Navarro, Frenk, & White 1996). This model of the galactic dark matter distribution was used for the neutralino-neutralino annihilation calculations of Bergström, Ullio, & Buckley 1997, henceforth BUB. They limited the analysis to a 1-sr cone along the line of sight to the galactic center to take advantage of the NFW enhancement.

In this analysis, GLAST was simulated in a somewhat simplified way using the GEANT program. (A more complete version of this calculation using the full GISMO Monte Carlo for the current GLAST baseline design is underway.) The geometric acceptance of the instrument was calculated for all gamma rays fulfilling the condition that a cylinder around the electromagnetic shower of more than eighteen radiation lengths and a radius of at least two Moliere radii is fully contained within the CsI calorimeter. This requires the gammas to enter at $>56^\circ$ from the normal on the front face of the instrument. This results in an energy resolution with $\sigma_E/E \sim 1.5\%$, assuming that the individual CsI crystals are carefully processed to allow uniform light collection along their length to $\sim 1\%$. Figure 2.b-5 shows a typical line shape (50 GeV) obtained from the GISMO Monte Carlo.

The rates for $\gamma\gamma$ and γZ annihilation depend on several unknown parameters in the MSSM. A systematic study of the MSSM phase space allowed by current experimental limits has been done in BUB. In addition, in this paper there are estimates of the diffuse galactic gamma-ray background, and the dark matter halo density function which are also needed to model the sensitivity of GLAST to the potential neutralino annihilation signal. Figure 2b-6 and Figure 2.b-7 show the results obtained by BUB for the GLAST cosmic neutralino discovery reach.

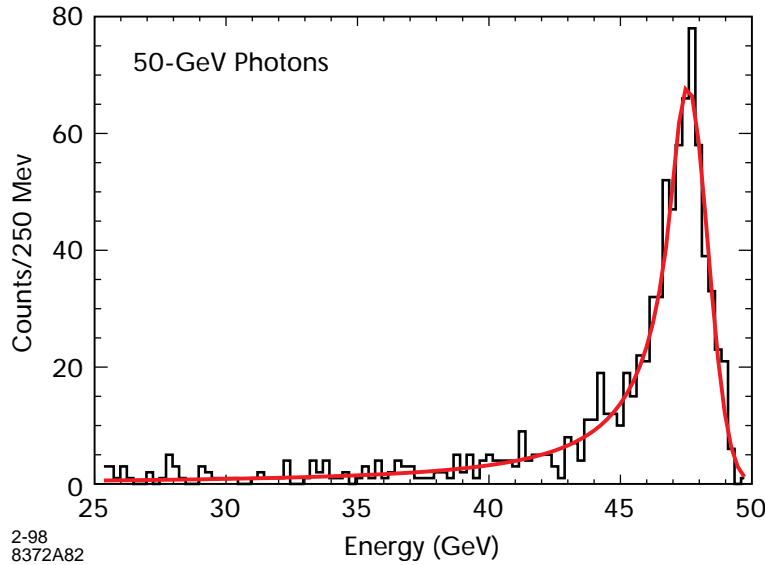


Figure 2.b-5 GISMO Monte Carlo calculation for 50-GeV photons entering the GLAST detector between angles of 56° to 90° to the front face normal of the detector. This angular range results in a greater than 18 r.l longitudinal path for the photon shower. Transverse fiducial cuts are also made in the calorimeter reducing the effective area somewhat, but resulting in a $\sigma_E/E \approx 1.5\%$ for high-energy gammas (obtained for each energy from a modified Gaussian line shape fit to the Monte Carlo distributions, shown in red in the figure for 50 GeV). The detector trigger is calorimeter only for these events. Note that BUB results presented in this document use the gamma energy resolution of 1.5% derived from the GISMO Monte Carlo, while the BUB transverse shower containment requirement of 2 Moliere radii is more severe than applied in the GISMO analysis.

The results shown in the figures are for two years in scanning mode; the various points sample the MSSM as described in BUB. The parameter, Z_g is the gaugino fraction defined for a neutralino. $Z_g < 0.01$ is higgsino-like, $0.01 < Z_g < 0.99$ is mixed, and $Z_g > 0.99$ is gaugino-like. The NFW galaxy dark matter halo profile giving the maximal flux has been assumed. The solid line shows the number of events needed to obtain a five-sigma detection over the galactic diffuse gamma-ray background as estimated from EGRET data (Hunter et al. 1997; Sreekumar et al. 1997). As the figures show, a significant portion of the MSSM phase space is explored, particularly for the higgsino-like neutralino for the $\chi\chi \rightarrow \gamma\gamma$ case.

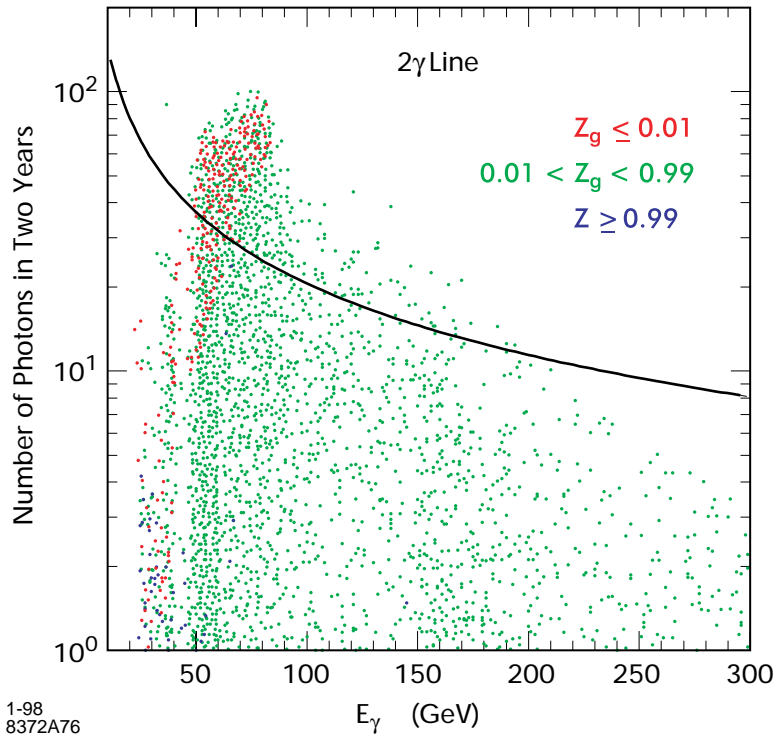


Figure 2.b-6 The number of events expected in GLAST for $\chi\chi \rightarrow \gamma\gamma$ from a 1-sr cone encompassing the galactic center, assuming a two-year scanning mode exposure and the Monte Carlo calculation described in the text. A different marker color is used for the three classes of neutralinos defined in BUB: a red marker indicates a higgsino-like neutralino, a green marker a mixed neutralino, while a blue marker indicates gaugino-like neutralinos. The NFW galaxy dark matter halo profile giving the maximal flux has been assumed. The solid line shows the number of events needed to obtain a five-sigma detection over the galactic diffuse gamma-ray background as estimated from EGRET data.

It should be noted that GLAST has a distinct advantage compared to ground-based detectors, such as air Cherenkov telescopes, if the halo contains a non-smooth, lumpy distribution of dark matter. From such regions the annihilation rates would be substantially enhanced, and the all-sky coverage of GLAST would not leave such “hot spots” undetected. There are theoretical reasons to expect such lumpiness (Silk & Stebbins 1993), and the dark matter-dominated dwarf spheroidal galaxies (Gilmore 1997) residing in the potential well of our galaxy could be lumps at the high-mass end of a distribution on all scales. In the estimates presented here, however, such enhancements of the rate are not included.

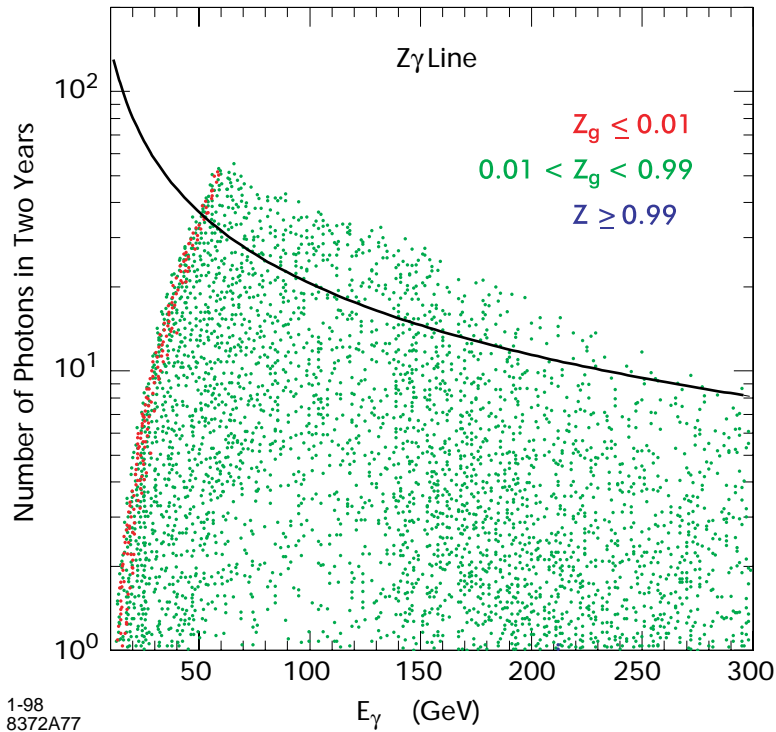


Figure 2.b-7 The number of events expected in GLAST for $\chi\chi \rightarrow \gamma Z$ from a 1-sr cone encompassing the galactic center, assuming a two-year scanning mode exposure and the Monte Carlo calculation described in the text. A different marker color is used for the three classes of neutralinos defined in BUB: a red marker indicates a higgsino-like neutralino, a green marker a mixed neutralino, while a blue marker indicates gaugino-like neutralinos. The NFW galaxy dark matter halo profile giving the maximal flux has been assumed. The solid line shows the number of events needed to obtain a five-sigma detection over the galactic diffuse gamma-ray background as estimated from EGRET data.

Of course, if there is a monochromatic gamma signal from $\chi\chi$ annihilations in the halo, there should in most cases also be an even larger continuum diffuse galactic component due to annihilations into quark jets. Although less resounding, this signal may also be detectable. Finally, it is very important to stress that neutralino annihilation is just an example of a source of monochromatic gamma rays. There could be other sources we have not yet imagined waiting for us to discover.

2.C Gamma-ray Bursts

2.C.1 Gamma-ray Bursts and GLAST

Cosmic gamma-ray bursts (GRBs) are intermittently the brightest sources in the gamma-ray sky. The peak fluxes of bright GRBs are 10^2 to 10^3 times more intense than the blazar AGNs detected by EGRET. The dimmest GRBs detected by BATSE, which will be visible to GLAST, are as bright as the Vela pulsar — the brightest steady gamma-ray source. GRB sources are now believed by virtually all astrophysicists to lie at cosmological distances. Thus the longest enduring mystery in modern astrophysics now appears to be the most fantastic, and still mysterious, physical phenomenon after the Big Bang itself: the implied radiant energy generated appears to be of order the gravitational energy available to a one solar rest mass object, $\sim 10^{51}$ ergs, or perhaps higher. GRB spectra tend to peak in $\nu F(\nu)$ within the 100-keV to 1-MeV regime, with power-law continuation past the electron-positron annihilation energy. This requires the emission region to be in bulk relativistic motion with Γ factors $\sim 10^3$. GRBs are therefore among the most powerful natural particle accelerators in the universe! Waxman, Kulkarni, & Frail (1997), propose that GRBs could be a significant source of cosmic rays up to 10^{20} eV. Also, Vietri (1997) suggests that GRBs could be a source of prompt (from the GRB itself) and delayed (from external shocks in an interstellar medium) neutrinos with energies $> 10^{19}$ eV.

Some appreciation of the chaotic and unpredictable nature of GRBs can be had from inspection of two GRB time profiles recorded by the BATSE and EGRET instruments on the Compton observatory. Figure 2.c-1 illustrates a very intense, short GRB whose wavefront just happened to pass the earth during the Superbowl of 1993 (Sommer et al. 1994). The true EGRET time profile is very uncertain because the EGRET dead time per photon is comparable to GRB pulse widths; hence, many more photons may have been incident on EGRET during the extremely intense initial pulse. Figure 2.c-2 shows another intense burst with very different temporal character which occurred in EGRET's field of view on Feb. 17, 1994. At BATSE energies (25–1000 keV), this event persisted for ~ 160 s; however, at EGRET energies, it apparently continued at a relatively high flux level past an Earth occultation, for at least 5000 s, to deliver a delayed ~ 18 GeV photon!

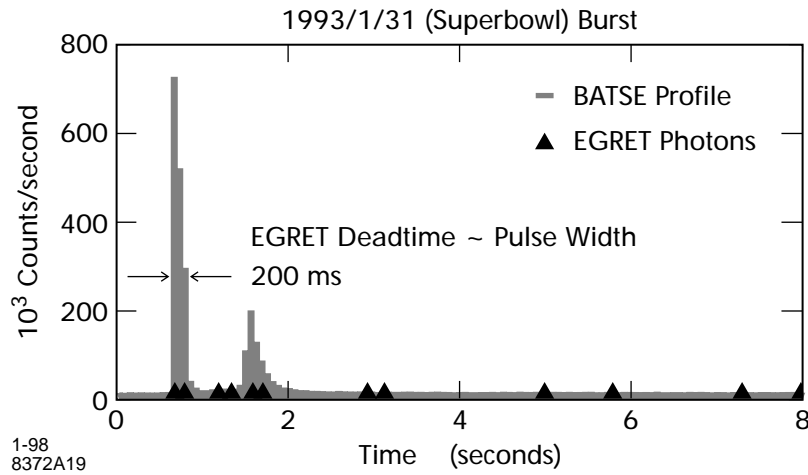


Figure 2.c-1 EGRET and BATSE light curves of the Superbowl burst, GRB930131. The burst consisted of an extremely intense spike, followed by low-level emission for several seconds. The true temporal development at energies >100 MeV is uncertain since EGRET dead time is comparable to GRB pulse widths.

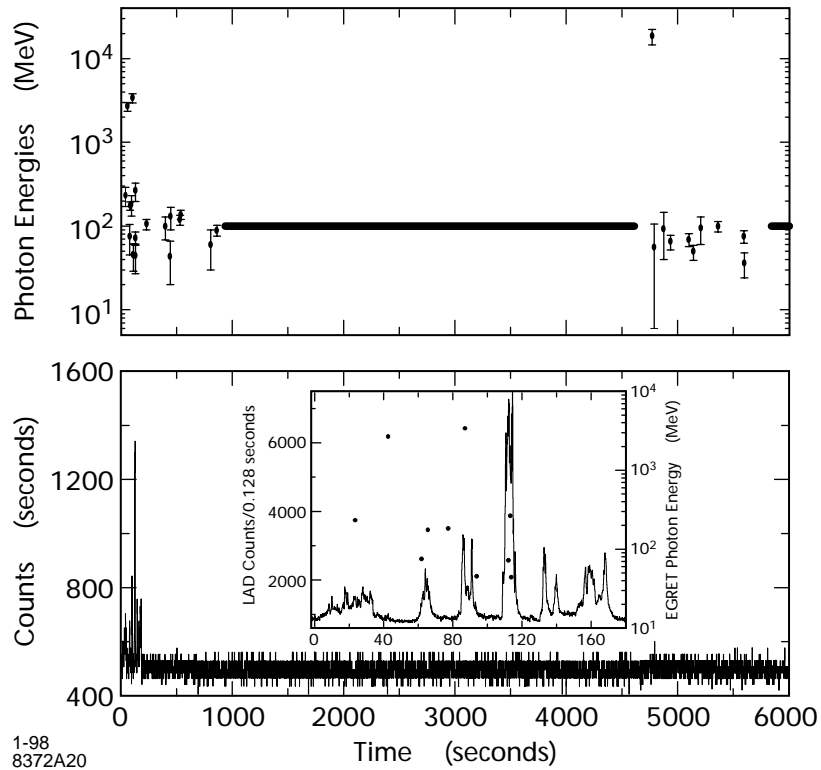


Figure 2.c-2 EGRET and BATSE light curves of GRB940217. Burst cessation at BATSE energies occurs at ~160 s. Extended emission at EGRET energies persists beyond an intervening earth occultation, up to 5000 seconds after the BATSE event.

The first exciting news for GLAST is that — reasoning from few events detected by EGRET, and from the distribution of GRB spectral power-law indices measured by BATSE and EGRET — GLAST with its negligible dead time, and increased area should detect virtually all GRBs in its large field of view (in other words, GLAST should “see the edge” of the GRB distribution, as does BATSE).

Second, and just as important, GLAST with negligible self-veto will have good efficiency above 10 GeV. The apparently common presence in bursts of 100-MeV to >10 -GeV photons means that GLAST will be able to localize GRBs with sufficiently high accuracy to enable rapid searches at all longer wavelengths — the “holy grail” of GRB studies. According to our Monte Carlo studies, perhaps half of the 200+ bursts per year detected by GLAST will be localized to better than a 10-arc minute radius, an easily imaged field for large-aperture optical telescopes.

2.C.2 Current Understanding

Since discovery by the Vela satellites in 1967 (Klebesadel, Strong, & Olson 1973), the GRB distance scale has been pushed past the solar system, the heliosphere and Oort cloud, the galactic disk, a putative extended galactic halo, the Local Group and metagalactic space, finally to the scale of the observable universe — at least for one burst. Figure 2.c-3 shows the results of a series of observations spanning the spectrum and executed in rapid succession from MeV energies to optical frequencies. These observations of GRB970228 have revealed power-law decay timescales in the x-ray (~ 1 day) optical (>7 months), as predicted for cosmological fireball models (Wijers, Rees, & Meszaros 1997).

The delayed emission at >100 -MeV energies mentioned above may now seem counterintuitive. Models have been proposed that account for the delay by increased cosmological path length of energetic pairs which upscatter microwave background photons (Plaga 1995), or by the original burst ejecta plowing into the ambient medium, generating external shocks (Meszaros 1997).

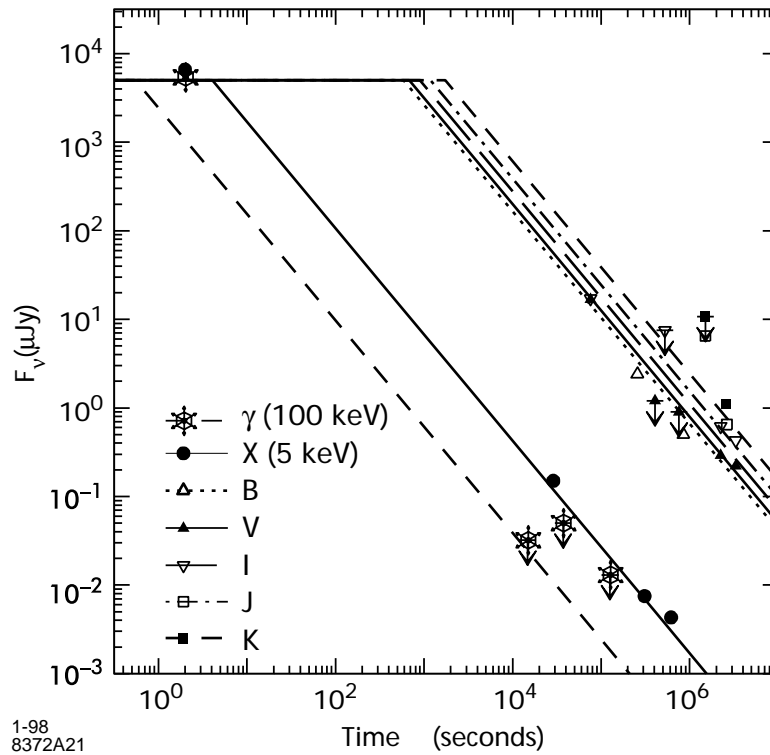


Figure 2.c-3 X-ray and optical light curves for GRB970228. Power-law decays, with timescales a function of frequency, characterize the presumed external shock phase, as predicted for cosmological fireball models.

Figure 2.c-4 shows the optical spectrum of the initial bright GRB970508 source which yielded the definitive signature: an absorption line system typical of a galaxy (Djorgovski et al. 1997), with redshift $z=0.835$, and an oxygen emission line (Metzger et al. 1997) with the same measure. This becomes the lower limit on distance for the source of GRB970508; the fading emission line suggests that this is the redshift of the GRB source. An extremely large energy reservoir is implied, of order a solar rest mass, uncertain by a factor of 100 or more.

As far as can be presently known from the few-degree-sized error boxes provided by BATSE for 2000 events, GRBs do not perform encores, and thus would appear to be singularly catastrophic explosions, possibly involving the complete transformation of a stellar mass.

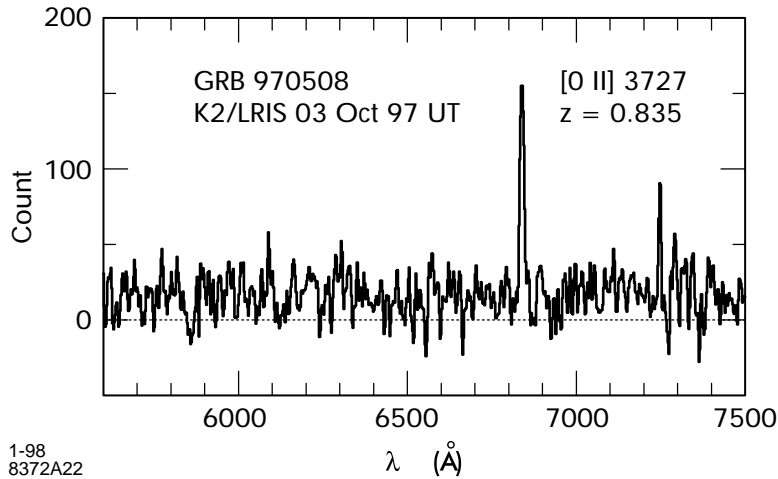


Figure 2.c-4 Optical spectrum of GRB970508, with absorption line system characteristic of high redshift galactic environment. GLAST's capability to localize GRBs to a few arc minutes will enable detection at all longer wavelengths.

Only one other optical counterpart has been found, that of GRB970228, and only a total of five confirmed x-ray afterglows have been detected by the BeppoSAX x-ray observatory (as of Jan. 22, 1998). However, statistical treatments indicate that probably all GRB sources lie at cosmological distances: the BATSE GRBs, and all subsets selected by spectral hardness or duration, have isotropic sky distributions. Isotropy combined with the inhomogeneous GRB intensity distribution (fewer dim GRBs are observed than would be present in a homogeneous distribution imbedded in an infinite Euclidean space) suggests a cosmological distance scale. The only other possible remaining distance scale, an extended galactic halo with a few hundred kiloparsec radius, is severely constrained by negligible dipole and quadrupole moments of the GRB distribution on the sky. Two additional statistical signatures are mutually quantitatively consistent with cosmic time dilation and concomitant redshift: on average, dimmer GRBs exhibit longer pulses and overall durations than do bright ones, and their spectral peaks are shifted to lower energies (Norris et al. 1994; Norris et al. 1996). The apparent time-dilation and redshift factor, $(1+z_{dim})/(1+z_{brt})$, found by comparing the redshifts of the brightest, z_{brt} , and dimmest bursts, z_{dim} , is of order two. But an absolute calibration of z_{brt} is yet to be obtained, and detailed considerations of the two optical counterparts, their presumed galactic hosts, and the near end of the intensity distribution complicate the distance scale picture.

2.C.3 Requirements for Investigating GRBs and GLAST Capabilities

From the above discussion it is clear that progress towards unraveling the GRB mystery is being made only by virtue of the multiwavelength detections and studies. However, a satisfying comprehension of GRBs will take many more years of observation. Approximately half of GRBs have associated x-ray decay tails; perhaps one fourth have optical counterparts. There is no evident correlation between GRB brightness and presence of an optical counterpart, whereas a redshift will be determined only for the brighter optical counterparts. Uncertainties in calibration of z_{brt} can only be resolved with the detection of many more optical transients since a GRB luminosity distribution rather than a “standard candle” seems more likely at this time. The interpretations of temporal stretching and shift of the spectral peak with dimmer GRB intensity as time-dilation and redshift, which if true would help calibrate GRB distances across their range in z , depend on calibration of z_{brt} . An optimistic estimate for the fraction of detected GRBs that will yield redshift determinations, given sensitivities of large optical telescopes (and assuming prompt access), is $\sim 1/30$, or ~ 10 per year (half-sky). The difficulty in attaining a calibration of z_{brt} will most likely be compounded by the large dispersion in GRB attributes. The dynamic range in GRB durations at ~ 100 keV is 10^5 , (10 ms– 10^3 s); we still do not have a good clue as to how this range can be so large while the range in spectral peak is only about one decade. We conclude that several years worth of GRB redshift determinations will be necessary to calibrate the distance scale.

Fortunately, reasoning from EGRET detections and BATSE spectra, GLAST will see ~ 200 – 300 BATSE-like GRBs per year, and will localize half of this yield to better than 10 arc minute radii, in near real time. GLAST's localization accuracy is competitive with, for example, the wide-field x-ray monitor of HETE-2 (10 arc min) and BeppoSAX (5 arc min), but its GRB yield will be much larger, by factors of ~ 6 and ~ 30 , respectively.

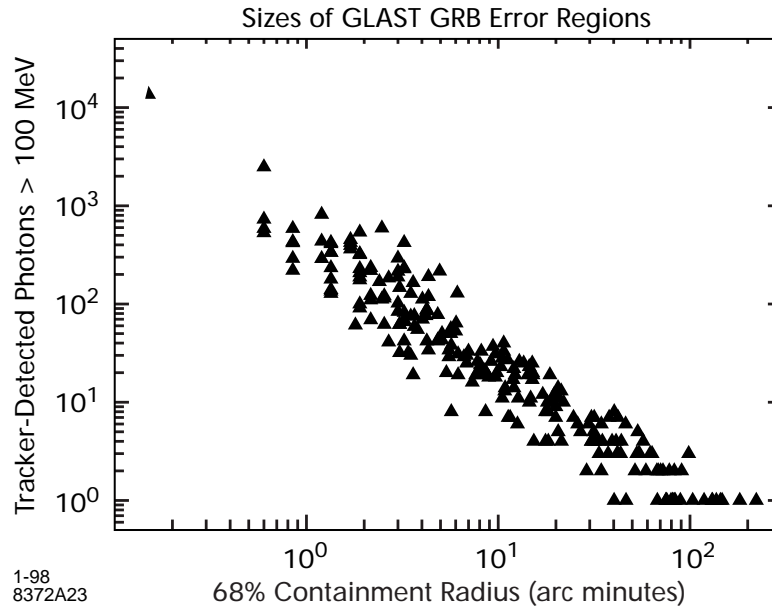


Figure 2.c-5 The GLAST 68% localization radii for GRBs with a spectral power-law index distribution $\alpha = 2.0 \pm 0.2$. The majority of localizations are determined to better than 10 arc minutes.

Figure 2.c-5 shows the power-law dependence relating the 68% localization error size versus number of GLAST tracker photons for one year's exposure. The limit of detectability at one tracker photon is obtainable for most bursts assuming a special 20 keV–10 MeV GRB trigger is possible. (This may require a separate GRB trigger instrument or an enhanced GLAST calorimeter trigger capacity). A low-power, low-weight monitor would signal the onset of an event and initiate a special real-time photon/charged particle discrimination mode.) The brighter half of detected GRBs, at fluences greater than ten tracker photons, are better localized and more likely to have detectable x-ray and optical counterparts. The simulations (Norris et al. 1997) assume scanning mode in low Earth orbit (~300 bursts above the horizon per year), and the current GLAST baseline design. Burst spectra were selected from a Gaussian power-law distribution ($\alpha = 2.0 \pm 0.2$) above 100 MeV, consistent with BATSE and EGRET detections (Band et al. 1993; Dingus et al. 1995; Catelli 1997); a fluence distribution proportional to the observed BATSE brightness distribution, and a brightness-independent duration distribution (Bonnell et al. 1997) spanning 0.1 s to ~500 s.

The present hodoscopic calorimeter design affords sufficient directionality and shower shape definition to discriminate against stiff cosmic rays. The

rejection power allows operation of the calorimeter, standalone, during medium- to high-intensity GRBs, and the detection of approximately three times as many photons as the tracker above 2 GeV. Figure 2.c-6 shows that the expected statistics for the brightest bursts are good enough to measure spectra to 100 MeV \rightarrow 100 GeV extending to the regime covered by ground-based Cherenkov observatories. Spectral cutoffs from ~ 10 GeV to 1 TeV may be generated by gamma-gamma attenuation by interaction of the GRB photons with the EBL background photons (Mannheim, Hartmann, & Funk 1996), as in the AGN case, and would be intensity- (redshift) dependent; cutoffs with no intensity dependence would constrain intrinsic models.

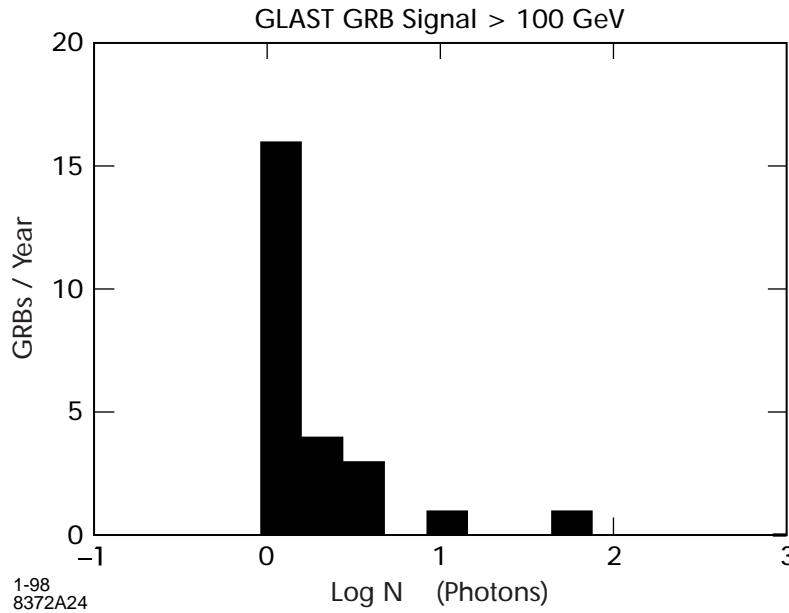


Figure 2.c-6 Assuming $\alpha = 2.0 \pm 0.2$, if GRB spectra continue up to 100 GeV, then ~ 25 bursts per year will be detected at that energy by GLAST, overlapping the spectrum to the regime covered by TeV ground-based observatories.

While the simulations illustrated in Figure 2.c-5 and Figure 2.c-6 are normalized to EGRET-detected bursts and cross-checked by extrapolations of BATSE spectra at ~ 1 MeV, BATSE's trigger accumulation criterion, integrated from 50 to 300 keV, does not allow it to see dim, spectrally hard bursts. Evidence for such events from Solar Max Mission's GRS (a small gamma-ray burst instrument) and Comptel, both with sensitivity to tens of MeV, were reported at the recent Fourth BATSE Symposium (Connors et al. 1997; Harris 1997). GLAST would be able to map the true spectral distribution of GRB, determining if these events represent a continuation of the known class or a distinct phenomenon.

In summary, GLAST will localize with good accuracy most if not all GRBs detectable in the optical regime, ~ 100 per year, enabling near real-time counterpart follow-ups at all longer wavelengths. Also, GLAST will study the GRB phenomenon with high temporal fidelity up to the highest energies expected to survive transmission through the intergalactic medium.

2.D Pulsars: Sources of Multi-TeV Gamma Rays

Pulsars, magnetized neutron stars whose rotation produces the characteristic pulsations, are unparalleled physics laboratories for many applications, as reflected by the fact that two Nobel prizes have already been awarded for pulsar studies. Nevertheless, some of the basic workings of pulsars remain unknown: How and where does the particle acceleration take place? What is the shape of the particle beam, and how is this energy converted to radiation? Where does the bulk of the energy go, since it is not seen in radiation? How do these fantastic astrophysical accelerators really work!

High-energy gamma-ray studies with GLAST will answer some of these fundamental questions. The six or more pulsars already seen by EGRET have set the stage for the GLAST observations. Except for transients, pulsars are the brightest sources in the gamma-ray sky. This is not true of any other branch of astronomy. Only in gamma rays can a significant fraction of the pulsar spin-down luminosity be seen. Pulsar models have changed dramatically to explain the observations, and these models make specific, testable predictions for GLAST.² Below we discuss some of the advances GLAST will make.

GLAST will find more gamma-ray counterparts of radio pulsars. Which radio pulsars are seen by GLAST will answer one of the basic questions about beam geometry and efficiency. If the apparent efficiency is largely a geometric effect, then GLAST should see radio pulsars whose magnetic and spin axes are fairly orthogonal, and not those that are aligned (Romani 1996). If the physics of particle acceleration and gamma-ray production determines the efficiency, then a different sample of radio pulsars will be seen by GLAST (Harding 1981). The factor of over 20 improvement in GLAST sensitivity for galactic plane sources compared to EGRET should produce dozens of radio pulsar detections, a large enough sample to distinguish the predictions.

GLAST will study the details of pulsar radiation. The phase-resolved energy spectra of the three brightest gamma-ray pulsars show a complicated pat-

² For a review of gamma-ray pulsar properties and models, see Thompson et al. 1997.

tern that is not explained easily by any model. The uncertainties are large, however, and the sample is small. GLAST will have the sensitivity and resolution to give detailed spectra for all the EGRET-detected pulsars and more. These spectra directly reflect the physics of gamma-ray production in the pulsar magnetosphere. Figure 2.d-1 shows that the shape of the observed high-energy cutoff, in particular, is a distinguishing feature of the present-day models. The vastly superior high-energy response of GLAST will give a definitive measurement.

Millisecond pulsars differ markedly from other pulsars in their fundamental parameters, and so occupy a unique position for studying particle acceleration and high-energy gamma emission from the pulsar magnetosphere. The luminosity of the hard x-ray pulsations detected from a millisecond pulsar is related to the spin-down luminosity just as that for known gamma-ray pulsars (Saito et al. 1997). This gives the expectation that GLAST will detect gamma-ray pulsations from several millisecond pulsars.

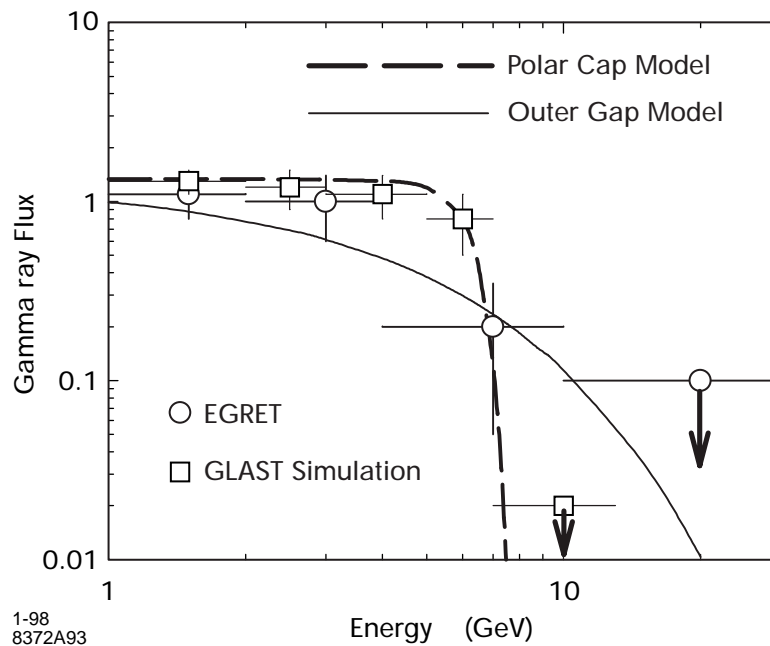


Figure 2.d-1 Modeled high-energy pulsar spectrum, showing the improvement in resolution between EGRET and GLAST. The polar cap model (Daugherty & Harding 1996) predicts a sharp high-energy cutoff, while the outer gap model (Romani 1996) predicts a more gradual cutoff. Unlike EGRET, GLAST will be able to distinguish the true shape of the spectrum (assumed to be that of the polar cap model in this simulation).

GLAST will also find more radio-quiet pulsars. Geminga, discovered in the x-ray band, is the first and most famous example of this type of pulsar. Additional radio-quiet pulsars have been discovered in the galactic plane in the hard x-ray band with ASCA (Torii et al. 1998; Vasisht & Gotthelf 1997). If there are many such pulsars, then gamma rays open a new window on the study of neutron stars and hence the supernova rate and distribution in the galaxy. What GLAST will do that EGRET could not is search for pulsations in the gamma-ray data, independent of radio or x-ray results. Only Geminga had a high enough photon density to allow such a search with EGRET. The combination of larger effective area and better angular resolution will give GLAST the capability of finding pulsations in *essentially all* of the unidentified EGRET sources, if they are radio-quiet pulsars. Mattox et al. (1996) discuss the method. For those sources too weak to be tractable with this method, GLAST offers a second possibility: the much smaller error boxes will permit deep-radio and x-ray searches for counterparts that might show pulsation, such as the thermal emission from the surface that allowed the detection of Geminga. Once a pulse period is known, even approximately, the gamma-ray data can be searched over a much smaller phase space than is required for a blind search. Conversely, the absence of pulsations in such sources would point to a new class of object and entirely different particle acceleration processes.

In addition to the directly accelerated particles that produce the pulsations, these rotating neutron stars can produce unpulsed emission through the pulsar wind. This wind, thought to consist of relativistic electrons and positrons, encounters the shock left by the supernova at some distance from the pulsar. The particles are further accelerated, to energies of 100 TeV or greater, and can produce very high-energy gamma rays through inverse Compton scattering. A number of these pulsar nebulae have been seen at TeV energies (Tanimori et al. 1997b). However, the emission does not extend to TeV energy in all pulsar nebula. This implies that the emission will cutoff in the GLAST energy band. Measurement of the cutoff energy is important because it is likely to be related to the maximum energy of electrons in the nebula. GLAST will provide two key bridges, one towards TeV Cherenkov telescopes and the other towards hard x-ray/soft gamma-ray satellite missions. In addition, GLAST will be sensitive to detecting protons accelerated by the nebula shock fronts, and thus exploring the origin of cosmic rays.

Pulsars were the first known gamma-ray source class. They remain an exciting field of study where GLAST will have guaranteed results.

2.E The Origin of Cosmic Rays

The origin of cosmic-ray particles is one of the most important unanswered questions in high-energy astrophysics. Cosmic rays are remarkable for a number of reasons. They span an enormous range of energies, from 1 MeV to more than 10^{20} eV. They are an important source of energy in the galaxy with an energy density comparable to that contained in the galactic magnetic field or in the cosmic microwave background. The sources which power the cosmic rays must have a total luminosity exceeding 10^{41} ergs/sec, and since the galactic containment time is estimated to be only $\sim 10^7$ years (Garcia-Muñoz 1977), the cosmic rays must be continually replenished during the lifetime of the galaxy.

Even after many decades of research, the exact origin of the very high-energy cosmic rays ($E > 10^{12}$ eV) remains unknown. In large part, our ignorance results from the fact that the bulk of the cosmic rays are charged and their trajectories bend in the inhomogeneous magnetic field of the galaxy. Any source information contained in the arrival directions of the particles at earth is lost. Photons are unaffected by magnetic fields and thus the observation of high-energy gamma-rays from point sources may identify the acceleration sites of cosmic rays.

There is evidence that shock acceleration in supernova remnants (SNR) offers a plausible explanation for cosmic-ray origin up to 10^{14} eV (Blandford and Eichler 1987, Axford 1994). This evidence is based on energetics and on theoretical models of shock acceleration which naturally lead to a power law energy spectrum for the accelerated particles (Legage and Cesarsky 1983), as well as some experimental corroboration of these ideas. Cosmic-ray electrons accelerated at SNR shock fronts emit synchrotron radiation; when the electrons have very high energy, > 100 TeV, the synchrotron radiation spectrum extends to the hard x-ray band. The first such hard x-ray signature observed from an SNR was by ASCA from SN1006 (Koyama et al. 1995). The wide-band spectrum from radio to hard x-rays delineates the predicted spectrum of synchrotron radiation very well. Since then similar signals have been observed by ASCA from other SNRs, such as Cassiopeia A.

Cosmic-ray protons accelerated by SNR shocks naturally interact with ambient matter either in the form of ejecta or material swept up from the interstellar medium. These interactions produce neutral pions which decay to gamma rays. Theoretical estimates of the expected gamma-ray luminosity of SNRs

have been carried out (Drury et al. 1994). These estimates indicate that gamma-ray measurements of sufficient sensitivity should provide additional evidence to support or contradict the SNR origin of cosmic rays. If SNR are the origin of high-energy particles, their gamma-ray spectra are expected to be harder than that of the galactic diffuse emission.

To date, gamma-ray measurements of SNRs have been inconclusive. EGRET observations indicate possible associations between several unidentified point sources near the galactic plane with known remnants (Esposito et al. 1996), but these associations are uncertain because of high levels of diffuse gamma-ray background and because of the poor angular resolution of EGRET. At very high energies ($E > 300$ GeV), atmospheric Cherenkov telescopes have so far failed to detect SNRs at sensitivity levels which are well below extrapolations from EGRET and are also below the initial theoretical expectations (Buckley et al. 1997). This result may imply a softening of the spectrum above EGRET energies which would be surprising in the context of the current models of shock acceleration.

NB: Recently, a tentative detection of the supernova remnant SN1006 in TeV gammas was reported (Tanimori et al. 1997). If confirmed, this result could be important for understanding the origin of cosmic rays.

GLAST will offer a significant improvement over EGRET in the study of SNRs, especially if GLAST data are combined with hard x-ray data expected from Astro-E (up to 600 keV), and XMM (up to 10 keV), as well as TeV gamma-ray data from ground-based Cherenkov telescopes. With its much improved angular resolution and flux sensitivity, GLAST will map the galactic diffuse emission on a fine angular scale which should allow the unambiguous identification of gamma rays from SNRs. In addition, the extended energy coverage of GLAST will permit the measurement of the SNR spectra to energies exceeding 100 GeV which should test whether SNRs are sources of high-energy cosmic rays.

In our galaxy, dense molecular cloud regions in the galactic plane, mapped out by the ^{12}CO surveys (see for example Matsuhara et al. 1997), provide enhanced target material for cosmic-ray interactions. Observations on small angular scales of gamma rays emitted by these clouds will allow the study of spatial variations in the cosmic-ray spectrum. The study of the nearby Magellanic clouds (LMC and SMC) also significantly impacts our understanding of cosmic rays. Gamma rays have been detected by EGRET from the LMC

(Sreekumar et al. 1993a) but spatial variations have not yet been measured. An upper limit to the gamma-ray flux from the SMC (Sreekumar et al. 1993b) has been interpreted as evidence that the bulk of the cosmic rays are galactic in origin, but more sensitive measurements by GLAST may allow for an actual detection of the SMC. GLAST observations of other sources, in addition to SNRs, may also have important ramifications for our understanding of cosmic-ray origins. Although SNRs are the only positively identified site of acceleration to the 100 TeV range so far, there are other sources where acceleration to a much higher energy may take place. Supernovae shocks and blazar jets are unlikely to power cosmic rays at energies above 10^{15} eV, and there is a great deal of speculation about the origins of these particles.³

There are several features to be satisfied for cosmic rays to reach the putative extreme high energies of $>10^{20}$ eV. Acceleration must take place over an enormous spatial scale, permeated by an adequate magnetic field for containment, having low material and photon densities, and using a long-lived shock front. Young pulsar nebulae, for example, the Crab nebula (Protheroe 1997), extended radio lobes of AGNs, and shock fronts in clusters of galaxies satisfy these conditions. In these cosmic accelerators, protons, electrons, and positrons will be accelerated. Electrons and positrons will then emit intense synchrotron radiation from the radio band to the lowest end of the GLAST energy range, ~ 100 MeV. At higher energies, GLAST will detect gammas from π^0 s produced by protons. Even if galactic sources, such as young pulsars, may have the energetics to accelerate particles to these extremely high energies, magnetic fields in the galaxy may not be able to provide the bending power to contain such particles (Hillas 1984). It is therefore generally speculated that the sources of extremely high-energy cosmic rays are extragalactic.

Gamma-ray observations by GLAST will be important in understanding the acceleration mechanisms occurring in AGNs and pulsars. These observations may provide further evidence to eliminate hadronic beam models in AGNs (Protheroe & Szabo 1992), which may in turn support an exotic origin for extremely high-energy cosmic rays (e.g., topological defects from the early universe).

³ Through studies of blazars, we now expect that the relatively large magnetic fields and high densities of photons in the jets prevent charged particles from reaching the highest energies in those sources.

2.F Ground-based Gamma-ray Experiments: Current Status and Relation to GLAST

High-energy gamma rays can be observed from the ground by experiments that detect the air showers produced in the upper atmosphere. Air shower arrays directly detect the particles (electrons, muons, and photons) in air showers, and atmospheric Cherenkov telescopes detect the Cherenkov radiation created in the atmosphere and beamed to the ground. Nitrogen fluorescence detectors, such as HiRes, also play a crucial role in detecting air showers, but only at much higher energies.

In the last decade, ground-based instruments have made great progress, both in technical and scientific terms. (For a recent review, see Ong 1997.) On the technical side, atmospheric Cherenkov telescopes have demonstrated that a high degree of gamma/hadron discrimination and a source pointing accuracy of 10–30 arc minutes (depending on the source strength) can be achieved based on the detected Cherenkov image. The Crab nebula, which has been shown to be a standard candle source at very high energies, can be detected with high statistical confidence in under twenty minutes of observation. The single-photon angular resolution achieved by the state-of-the-art Cherenkov telescopes such as Whipple, CANGAROO, CAT, or HEGRA approaches 0.1 degrees above 500 GeV. As one goes to lower energies with advanced telescopes, this measurement is expected to broaden by about a factor of two.

The technical advances made by atmospheric Cherenkov telescopes have led to important scientific results. There are now at least five gamma-ray point sources that have been detected with high statistical significance at energies above 250 GeV. These sources include three pulsar nebulae (Crab, Vela, and PSR B1706-44) and two extragalactic AGNs of the BL Lac class (Mrk 421 and Mrk 501). Recently, a tentative detection of the supernova remnant SN1006 was reported (Tanimori et al. 1997a); if confirmed, this result could be important for understanding the origin of cosmic rays. Figure 2.f-1 shows that the measurement of the unpulsed spectrum of the Crab nebula at very high energies provides strong support for the synchrotron self Compton model of acceleration in the nebula (De Jager et al. 1996).

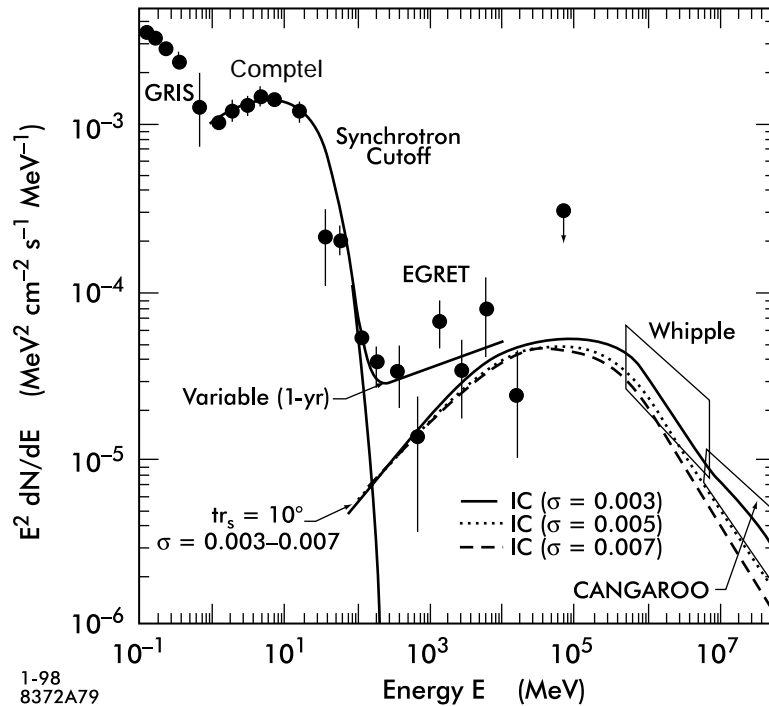


Figure 2.f-1 The Crab nebular unpulsed gamma-ray spectrum ($E^2 dN/dE$) in the energy range 0.1 MeV to 20 TeV (De Jager & Baring 1997). A two-component fit (1–150 MeV) resulted in a power law with an exponential cutoff at 25 MeV, and an inflection point at 150 MeV. Inverse Compton scattering was used to generate the high-energy component to 20 TeV. The model is uncertain by a factor of two at any energy.

The ground-based gamma-ray community is growing quickly and a number of new experiments are under construction or in the proposal stage. MILAGRO is a large, water Cherenkov detector that will be the first air shower array to operate at energies below 1 TeV (Berley et al. 1997). Starting in 1998, MILAGRO will make the first all-sky survey at very high energies. The STACEE (Chantell et al. 1997) and CELESTE (Quebert et al. 1997) experiments, currently under construction, will use large heliostat mirrors at solar energy facilities to collect a much larger fraction of the Cherenkov radiation in gamma-ray air showers than conventional Cherenkov telescopes. The large collection areas may allow these experiments to make the first ground-based observations in gamma-ray energy region between 50 and 250 GeV. Finally, the success of the Whipple and HEGRA experiments have led to the design of new Cherenkov telescopes consisting of arrays of imaging reflectors. Two such telescopes are in the development stage: VERITAS (Weekes et al. 1996) and HESS (Aharonian et al. 1997). If fully approved, operation of these experiments could start as early as 2002. Figure 2.f-2 shows a comparison of sensitivity of the various techniques (Weekes et al. 1996).

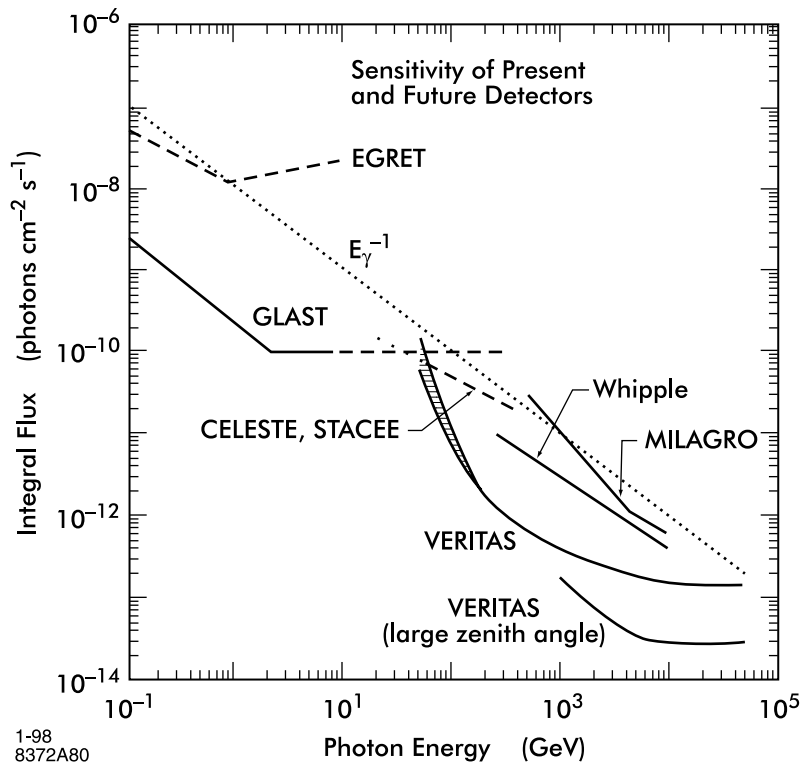


Figure 2.f-2 The predicted sensitivity of a number of operational and proposed ground-based Cherenkov telescopes — CELESTE, STACEE, VERITAS and Whipple — for a 50-hour exposure on a single source. EGRET and GLAST sensitivity is shown for one year of all-sky survey. MILAGRO sensitivity is shown for one year of sky survey. Note the excellent overlap region between GLAST and a number of the future telescopes. This should allow a very accurate energy/sensitivity calibration to be made for the ground-based instruments in the 50-GeV to 1-TeV energy range, for example via simultaneous observations of the Crab nebula (Weekes et al. 1996, excepting GLAST sensitivity).

The detections of Markarian 421 (Punch et al. 1992) and Markarian 501 (Quinn et al. 1996) illustrate the important complementarity of ground-based instruments with satellite measurements: during this same time period, EGRET was unable to detect a signal from Mrk 501 (even though it has detected about 50 AGNs compared with two by the ground-based experiments). This was due to a lack of EGRET sensitivity. Figure 2.f-3 shows the hard spectrum for very high energy seen by the CAT detector (Protheroe et al. 1997). For Mkn 501 there appears to be a dip in the spectrum in the 100 MeV range (Protheroe et al. 1997), implying in a Compton-synchrotron model that the electrons have very high energies. As GLAST's sensitivity will be about two orders of magnitude higher than EGRET's, and GLAST will have

a considerably expanded energy range to high energy, it may be possible for GLAST to measure the structure of this dip region in some detail, further testing these types of models.

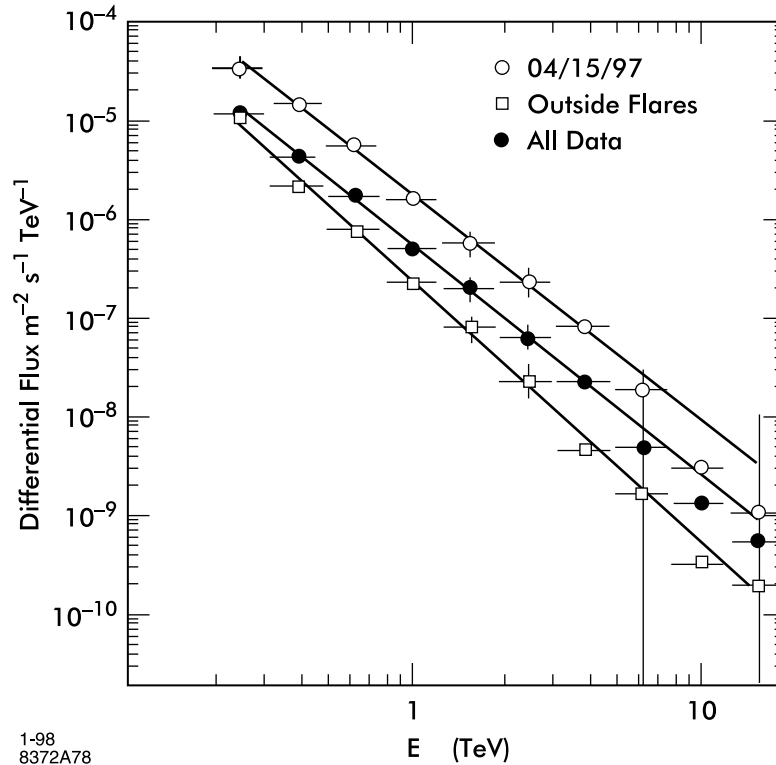


Figure 2.f-3 Preliminary CAT measurements of energy spectrum from Mkn 501 (Protheroe et al. 1997). The differential flux vs. energy has a hard behavior from $0.25 \text{ TeV} < E < 10 \text{ TeV}$, with a slope of about 2.45 ± 0.2 .

Ground-based detectors, particularly atmospheric Cherenkov telescopes, have very large collection areas ($>10^8 \text{ cm}^2$), excellent angular resolution, and good energy containment at very high energies (26 radiation lengths). These detectors also have drawbacks, including low duty cycles (10%), small fields of view (<5 degrees), moderate energy resolutions (25%) with systematic energy and sensitivity calibration uncertainties, and poor capabilities for observations of extended or diffuse sources.

By contrast, GLAST has a very large field of view, highly efficient duty cycle, and a wide energy range from 20 MeV to greater than 300 GeV with excellent energy resolution and low systematic energy calibration uncertainties. Thus, GLAST will operate in an almost totally complementary manner to ground-based instruments. GLAST is particularly well suited for all-sky moni-

toring of transient point sources, observations of diffuse sources, and for the rapid discovery of new phenomena. Its capabilities are also important for the greater success of ground-based instruments.

For individual point sources, ground-based instruments have unparalleled sensitivity at very high energies (above 50–250 GeV), and thus can provide important additional information. For many objects, full multi-wavelength coverage over as wide an energy range as possible will be needed to understand the acceleration and gamma-ray production mechanisms. In addition, at high energies above ~ 10 GeV the spectra from distant AGNs may be cut off due to absorption by interstellar radiation fields (see Figure 2.a-8, page 2-13). Spectral measurements by both GLAST and ground-based instruments will be needed to measure these absorptive effects accurately.

In summary, ground-based gamma-ray experiments study a number of astrophysical sources that are of interest to GLAST, and in a complementary manner. These experiments have made significant progress over the last ten years. The success and continued development of the ground-based community therefore greatly enhances the scientific merits and rationale for GLAST and vice versa.